NASA Technical Paper 1678

Single-Stage Electrohydraulic Servosystem for Actuating an Airflow Valve With Frequencies to 500 Hertz

John A. Webb, Jr., Oral Mehmed,
and Carl F. Lorenzo

AUGUST 1980

NASA

NASA Technical Paper 1678

Single-Stage Electrohydraulic Servosystem for Actuating an Airflow Valve With Frequencies to 500 Hertz

John A. Webb, Jr., Oral Mehmed,
and Carl F. Lorenzo
Lewis Research Center
Cleveland, Ohio

National Aeronautics
and Space Administration

**Scientific and Technical
Information Branch**

1980

Summary

An airflow valve and its electrohydraulic actuation servosystem are described. The servosystem employs a high-power, single-stage servovalve to obtain dynamic response beyond that of systems designed with conventional two-stage servovalves. A detailed analysis of the electrohydraulic servosystem is presented, along with a discussion of the limitations imposed on system performance by such nonlinearities as signal saturations and power limitations. The relationship for selecting optimum actuator piston area for this servosystem was determined by using equations derived from an analysis of system limitations.

Details of the mechanical design of both the actuator and the airflow valve are presented. Because of the high-frequency operation of this valve, a NASTRAN analysis of the moving element in a slotted-cylinder airflow valve was used to insure the structural integrity of the hardware. The fixed element in the airflow valve was coated with a unique solid lubricant to prevent excessive wear and galling between moving surfaces. Other special design features required by this application are briefly described.

Dynamic data are presented in the form of sweep-frequency test results, plotted as amplitude and phase versus logarithimic frequency. Experimental transfer function data are presented for portions of the actuator position-control servo-system. Overall position-response data are compared with results from a limit-line analysis as well as with a detailed analog computer model.

The servosystem described in this report exhibited a dynamic response of -3 decibels at 490 hertz for excitation amplitudes of 20 percent of full stroke (where full stroke corresponds to 0.635 cm or an airflow-valve area of 40 cm^2) with a 1.1-kilogram (2.5-lb) inertia load. The airflow valve was used successfully to determine the airflow dynamics of a six-stage, axial-flow compressor and in closed-loop control investigations of compressor stability.

Introduction

Investigations aimed at providing a better understanding of the high-frequency dynamics of turbojet engines require data generated by high-frequency perturbation devices. These data can be used to upgrade models used in the design of engine control systems. High dynamic response may also be required to provide stabilizing controls that must be sufficiently fast to compensate for unstable flow phenomena. In the past, servopositioned air valves have been used for the investigation of turbojet engine dynamics (refs. 1 to 4), airflow distortion (ref. 5), and inlet control systems (refs. 6 and 7). Most of these valves used the conventional two-stage electrohydraulic servovalve to obtain dynamic capabilities to 200 hertz (ref. 8).

An investigation of unstable flow phenomena associated with compressor surge required an airflow-modulating valve with a high dynamic response capability. The use of this valve would be twofold: as a disturbance device for determining the dynamics of the compressor, and as a control element for studying methods for stabilizing unstable flow phenomena. The dynamic response requirements for stabilization controls were determined analytically to be beyond the capabilities of conventional two-stage electrohydraulic servovalves. In addition, the airflow valve had to be close coupled physically to a primary, annular airflow passage while passing a secondary (uncontrolled) airflow out of the duct formed by the core of the primary annulus. Moderate airflow leakage at closure and minimum structural coupling with the compressor casing were additional constraints.

The servosystem designed to meet these requirements employed a single-stage servovalve. The maximum dynamic response obtainable from an electrohydraulic servosystem is set by basic power and flow limitations and the linear dynamics of the servovalve and actuator. The effect of hydraulic power and flow limitations can be minimized by optimizing the actuator piston area (refs. 9 and 10). The hydraulic resonant frequency can be maximized by minimizing the actuator cavity volumes and the moving-element mass. By eliminating the first stage employed in conventional servovalves and driving the spool valve directly from a high-power coil driver, the first-stage flow limit is eliminated and the linear dynamics can be extended. The type of single-stage servovalve used in this application had been used primarily on large hydraulic shaker equipment.

This report describes the airflow valve and its electrohydraulic servosystem. Presented are a description of the airflow-valve servosystem, an analytical derivation of a nonlinear analog model of

the servosystem, nonlinear performance limit criteria, comparison of experimental results with the model, and developmental considerations. Sweep-frequency data for internal system transfer functions that were used to verify the model are presented. Closed-loop frequency response data for various excitation amplitudes are presented to demonstrate the effect of nonlinear limits on system performance. These results are compared with the analog computer model.

The airflow valve provides a full flow area of 40 square centimeters with a total actuator stroke of 0.635 centimeter (0.25 in.). The actuator was designed to drive an air valve weighing 1.1 kilograms (2.5 lb) to frequencies of 500 hertz with a 2068-N/cm^2 (3000-psi) hydraulic supply pressure.

Airflow-Valve Servosystem

Design Requirement

The airflow valve was designed to provide a controlled compressor exit area for a small, six-stage, axial-flow compressor that was driven by an air turbine (ref. 11). The compressor exit flow was ducted through an outer annular passage while the turbine exhaust flow exited a center or core passage. As a test device for studying compressor characteristics the airflow valve had to control the annular compressor flow while providing an open exit flow path for the core turbine exhaust.

The design requirements for the airflow valve, its hydraulic actuator, and the control system are presented in table I. The airflow-valve requirements were set by the design operating point of the compressor. A slotted-cylinder configuration was chosen for the airflow valve, and the resulting slot sizes were determined by airflow and servosystem considerations. The moving-element clearance requirement was dictated by the minimum leakage flow allowable at full closure. The maximum acceleration force that the airflow valve must tolerate was set by the maximum pressure-area force of the actuator, but the deceleration force can exceed the acceleration force and is particularly large in the event of an actuator end-cap impact. The structural design of the airflow-valve moving element is influenced by these impact forces. This creates a design trade-off between moving-element mass, end-cap cushions, and the effect of these two on the servosystem response.

The design requirements for the hydraulic actuator were set primarily by system dynamic considerations. The piston area was determined from nonlinear response-limit considerations. This resulted in an optimum piston area, as discussed in the section Nonlinear Performance Limits. Because of the nonlinear limits on system performance, the piston position-response bandwidth decreased as the stroke amplitude increased. Therefore the maximum piston stroke was specified to meet the dynamic response requirements. The moving-element mass and the hydraulic fluid volume requirements were chosen to provide a hydraulic resonant frequency beyond the predominant linear dynamics of the servosystem. However, the volume requirement was not met because of the large cavity volumes in the electrohydraulic servovalve control ports. This situation was compensated for by reducing the final design moving-element mass below the specified amount.

The control-system dynamic response requirements are also shown in table I. They were determined from the application requirements of the airflow valve.

Airflow-Valve Servosystem

The airflow valve and its servoactuator are shown in figure 1. The servoactuator was mounted on a T-slot bedplate on the floor of a test cell for preliminary response testing. The slotted-cylinder

TABLE I. – DESIGN REQUIREMENTS FOR AIRFLOW VALVE

Airflow valve:	
Maximum pressure difference across valve, N/cm^2	35
Maximum airflow through valve, kg/sec	1.5
Full open flow area, cm^2	39
Valve shot width, cm	0.635
Valve moving-element clearance, cm	$\leq$0.010
Maximum operating pressure drop, N/cm^2	34
Maximum operating temperature, K	400
Area-to-stroke linearity, percent	1
Maximum acceleration force, N	6700
Maximum deceleration force, N	6700 (plus actuator end-cap impact force)
Valve flow configuration	Controls annular flow area and provides open exit flowpath for core turbine exhaust
Hydraulic actuator:	
Piston area, A_v, cm^2	2.96
Maximum piston stroke, $X_{v,max}$, cm	0.635 (plus $\geq$10 percent)
Moving-element mass, M_v, kg	$\leq$1.8
Servovalve supply pressure, P_{su}, N/cm^2	2068
Hydraulic fluid volume, V_t, cm^3	$\leq$10 (includes actuator, porting, and servovalve control ports)
Control system:	
Valve-position amplitude response to 200 Hz, dB	$\pm$3
Valve-position phase response at 200 Hz, deg	-90

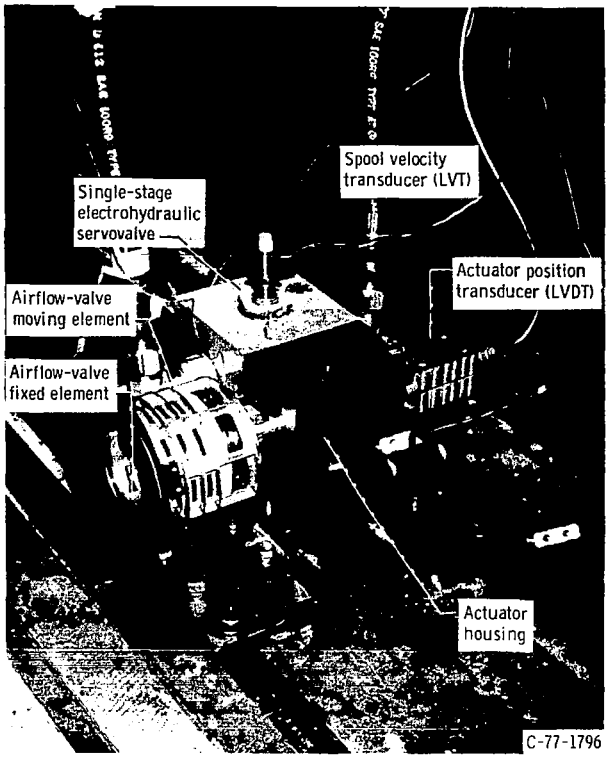

Figure 1. - Airflow valve and servoactuator - floor mounted.

design had an outer moving element that was positioned by the actuator and an inner fixed element that was supported by a ring mounted to the actuator block. Compressor airflow exited through the slots. The actuator piston was driven by a single-stage, electrohydraulic servovalve whose spool-valve velocity was measured with a linear velocity transducer (LVT). The piston position (or airflow-valve area) was measured with a linear, variable differential transformer (LVDT).

A schematic diagram of the airflow valve, its actuator, and the servosystem for positioning the valve is shown in figure 2. The flow paths for the compressor and turbine are shown in the cross-sectional view of the airflow valve. The piston position signal from the LVDT was fed into an electronic controller, where it was differenced with a precompensated command signal and a manual set-point signal (used for steady-state positioning). The precompensator was a second-order lead-lag circuit designed to extend the linear response of the servosystem. The error signal was amplified and applied to a power amplifier that was used to drive the coil on the electrohydraulic servovalve. An internal feedback loop provided current feedback to help extend the amplifier-coil dynamics beyond the resistive-inductive impedance of the coil.

The electrohydraulic servovalve was a single-stage, four-way spool valve positioned mechanically by the sum of the forces exerted by the springs at either end of the spool and the current-driven coil. The spool valve ported hydraulic supply and return pressures into the actuator piston chambers to position the piston. The second-order dynamics of the spool mass suspended by springs were very lightly damped, and the presence of small flow forces on the spool were sufficient to excite this resonance. Therefore velocity feedback was required to provide sufficient damping to insure stable operation. This damping was provided by the LVT mounted at the right end of the servovalve spool in figure 2. The output signal of the LVT was fed into a feedback compensator, which was essentially an integral-plus-proportional feedback, to push the spring-mass resonance to a higher frequency and to provide added damping.

Applications

The airflow valve must perform two functions: one for compressor perturbation studies, and the other for closed-loop compressor control. The airflow valve mounted in the test chamber is shown in figure 3. Figure 3(a) shows the airflow valve used as a termination for an airflow duct (cold pipe) mounted in the location where the compressor would normally be placed. With airflow passing through the duct the valve can be oscillated to provide dynamic data for identifying the duct dynamics of the upstream piping. These data were obtained from dynamic pressure and flow instrumentation stations, as shown. Only perturbation testing was done with this configuration.

When the six-stage, axial-flow compressor was mounted on the stand, the test rig appeared as in figure 3(b). Here the compressor is obscured by the stage instrumentation lines. Exit airflow directions are shown in the figure. In this configuration both dynamic perturbation and stabilization controls tests were performed.

A block diagram depicting the use of the airflow valve as a stabilizing device is shown in figure 4. The airflow-valve-area feedback loop (or piston position loop) became an internal loop with an outer loop formed by feeding back the dynamic measurements of the airflow process. Although the compressor airflow process dynamics at some operating points were unstable, they could theoretically be stabilized with the proper feedback signals and feedback compensation network. The output of the feedback compensator provided a dynamic command signal for airflow-valve area.

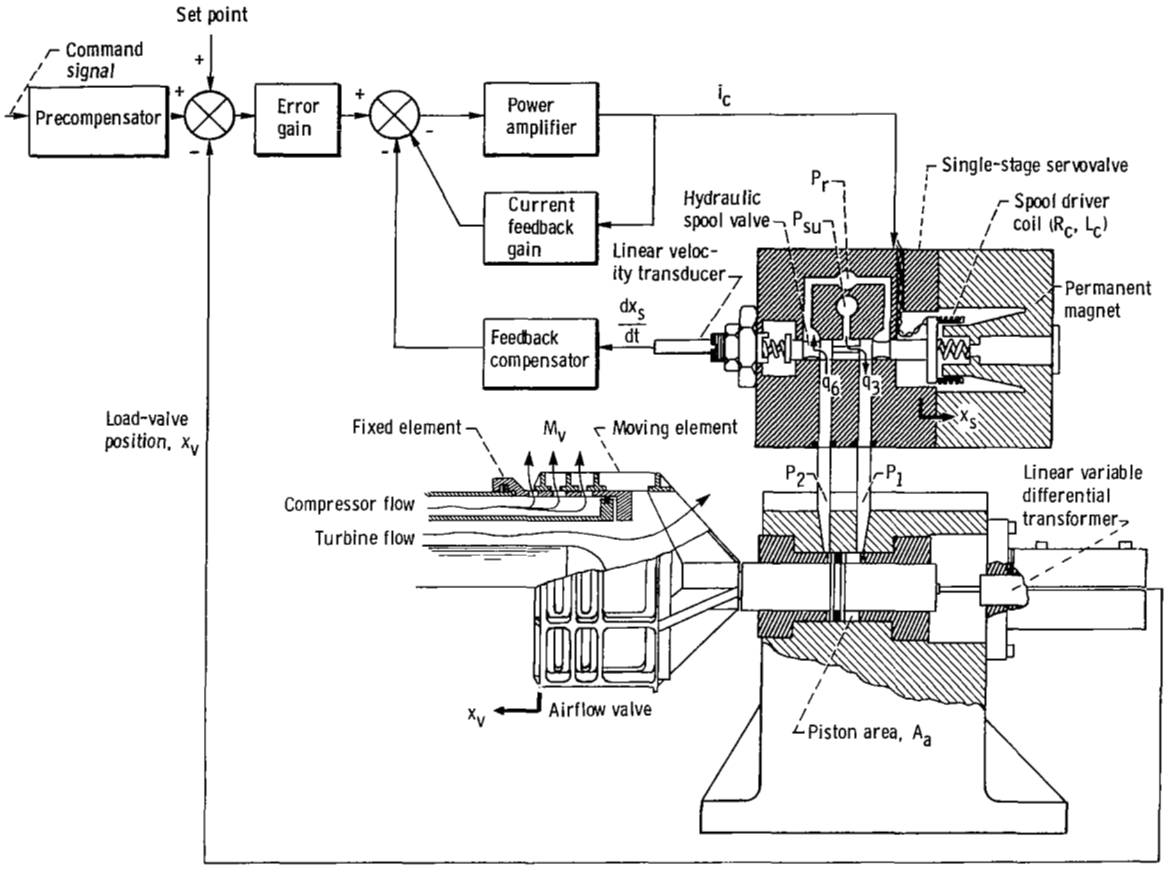

Figure 2. - Schematic of electrohydraulic servosystem for positioning airflow valve.

Mechanical Design Features

The airflow valve and its servoactuator were designed to provide long-term reliability during high-frequency, experimental sweep-frequency response testing, in addition to meeting the requirements of table I. This section of the report describes the physical hardware and discusses design decisions.

Airflow-valve servoactuator.—An overall view of the disassembled airflow-valve servoactuator is shown in figure 5(a). The three primary sections of the airflow valve itself were the fixed element, the moving element, and the fixed-element support ring. The support ring was slotted to provide a path for the moving-element struts when they were assembled. One pair of guide rollers was mounted on the fixed-element support ring to prevent rotation of the moving element. These rollers were not preloaded and were intended only to provide a rolling guide to prevent piston rotation.

The actuator piston had a tapered rod at one end to provide a mounting attachment to the moving element. The moving element had a tapered hole and was held on the rod with a self-locking nut. This provided a backlash-free union between piston and moving element that could not be loosened by mechanical vibration. The piston was supported by the two bronze end caps, which fit into the ends of the actuator-block bore. The actuator-piston position transducer (LVDT) was housed in an aluminum block that had heating elements cemented to it. The heaters were controlled to maintain a constant LVDT temperature in order to eliminate thermal drift problems. The temperature was measured with a small sensor embedded in the side of the LVDT mounting block. The electrohydraulic servovalve is shown with a cover plate over its control ports. A case accelerometer was mounted on the servovalve housing to measure vibration in the vertical axis.

The reverse side of the actuator block is shown in figure 5(b). The servovalve mating surface had a dowel pin to insure proper alinement of the servovalve control ports with respect to the actuator-

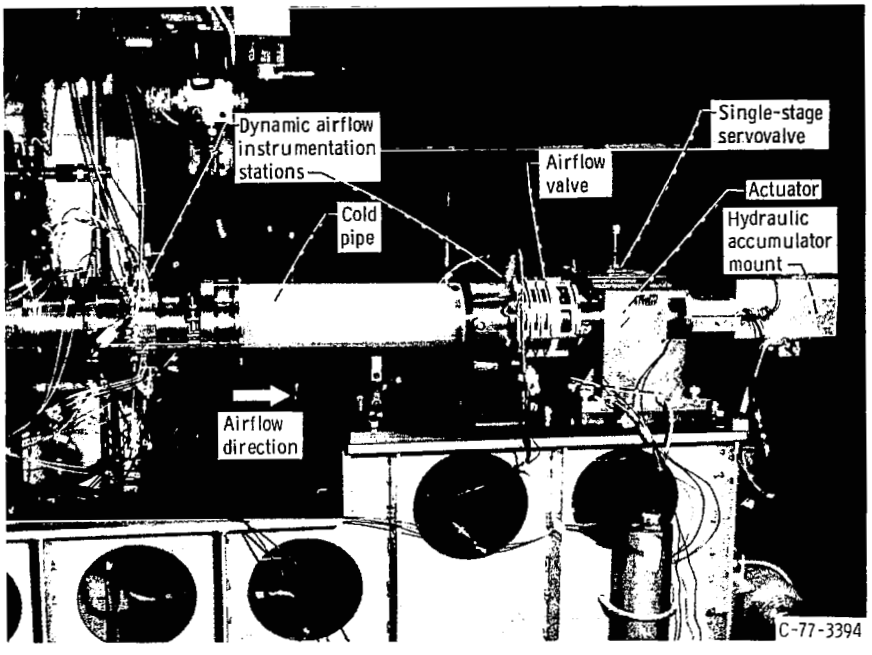

(a) Cold-pipe-mounted airflow-valve for duct dynamics test.

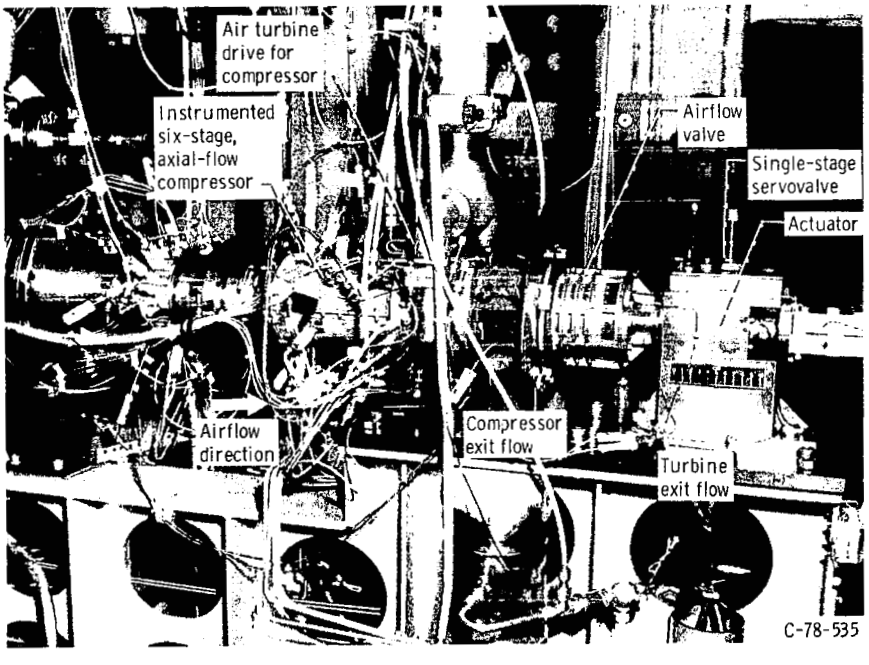

(b) Airflow-valve used as compressor exit area for dynamics and controls studies.

Figure 3. - Applications for airflow valve.

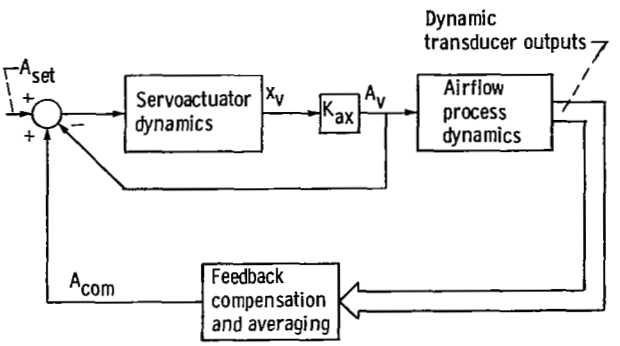

Figure 4. - Use of airflow valve as stabilization device.

block control ports. Each actuator-block control port was drilled at a compound angle to provide a 90° shift in orientation from the servovalve-spool axis to the piston axis. This minimized the flow-path resistance and fluid volume for these ports.

The bronze end caps provided a bearing surface for the actuator-piston rod. A double inner seal was obtained between the end caps and the piston by using Teflon rings backed by cap-rings (insert in fig. 5(b)). These seals were located at the outer edge of the end cap to provide a relatively long bearing surface. Since the piston rod was supporting a cantilevered load mass, these bearing surfaces saw greater side loads than in conventional actuator designs. The surface was lubricated with oil from the piston chambers by means of oil feed grooves in the bearing surface along the axis of piston motion. A pressure-equalizing groove was located just before the inner seals. The end caps were sealed to the actuator-block bore with O-rings and a Teflon backup ring. An oil drain was provided to prevent oil leakage at the piston rod ends. The actuator piston was sealed to the bore with split Teflon piston rings backed by a corrugated spring. Thermocouples were installed in the end caps as near as possible to the bearing surface to monitor lubrication effectiveness via the bearing temperatures during high-frequency motion.

Single-stage, electrohydraulic servovalve.—The dissassembled single-stage, electrohydraulic servovalve is shown in figure 5(c). This unit, a commercially available device (ref. 12), had been used primarily in vibration testing equipment. As a general-purpose industrial device this valve was designed for a wide range of flow rates. The maximum flow rate was set by the maximum coil current $E_{pa,sat}$ and the selected spring rate K_{sp}. Low spring rates provide high flow rates but with a penalty of decreased dynamic response. For the relatively small actuator needed for the airflow valve, the high flow rates were not necessary. Therefore this design used stiff springs to achieve a high-frequency spring-mass resonance. However, the large control ports in the servovalve contained an excessive volume of oil that degraded the hydraulic fluid-spring to actuator-mass resonance. To decrease this volume, aluminum plugs were inserted into the control ports of the servovalve as shown in figure 5(c). The plugs were drilled through with a smaller diameter hole to pass the control-port flows.

Another modification was the addition of a spool velocity transducer. The null adjusting screw mounted in the end cap of the servovalve (to right in fig. 5(c)) was drilled through to allow insertion of the velocity transducer, which was held in place with set screws. The permanent-magnet core of the transducer was mounted to the upper-spring retainer. The velocity transducer was mounted in this manner to provide ease of access for replacement or repair. It also placed the LVT sufficiently distant from the strong servovalve permanent magnet to avoid magnetic effects on the LVT core.

Airflow-valve design.—The airflow valve consisted of two concentric, cantilevered assemblies, as shown in figure 6. The valve moving element was mounted on the piston rod to make the outer cantilevered assembly. The valve fixed element, together with its support ring, was mounted on the actuator housing and made up the inner cantilevered assembly. The fixed and moving elements were slotted cylindrical structures. The relative slot positions determined the amount of airflow through the valve. The slot positions were controlled by piston position, as shown in the cross-sectional view of figure 7. The valve and its actuator were designed as an integral unit separate from the turbojet simulator duct for ease of testing and development. The cantilevered arrangement was used to minimize mechanical complexity and to eliminate the need for antifriction bearings between the fixed and moving elements. A pair of cam rollers, shown in figure 7, were used as an antirotation device to maintain the alinement of the slots between the valve fixed and moving elements. An eccentric shaft on each cam roller was adjusted to leave about 0.127-millimeter (0.005-in.) of free play between the moving-element strut and the rollers.

A pair of elastomeric seals between the valve fixed element and the turbojet simulator duct served a dual purpose. They sealed the compressor flow cavity and provided a flexible coupling between the valve assembly and the turbojet simulator duct.

The small clearance between the surfaces of the fixed and moving valve elements, which was necessary to minimize airflow leakage, required the use of a surface coating. The coating prevented galling between these surfaces if contact occurred during high-speed oscillation of the moving element.

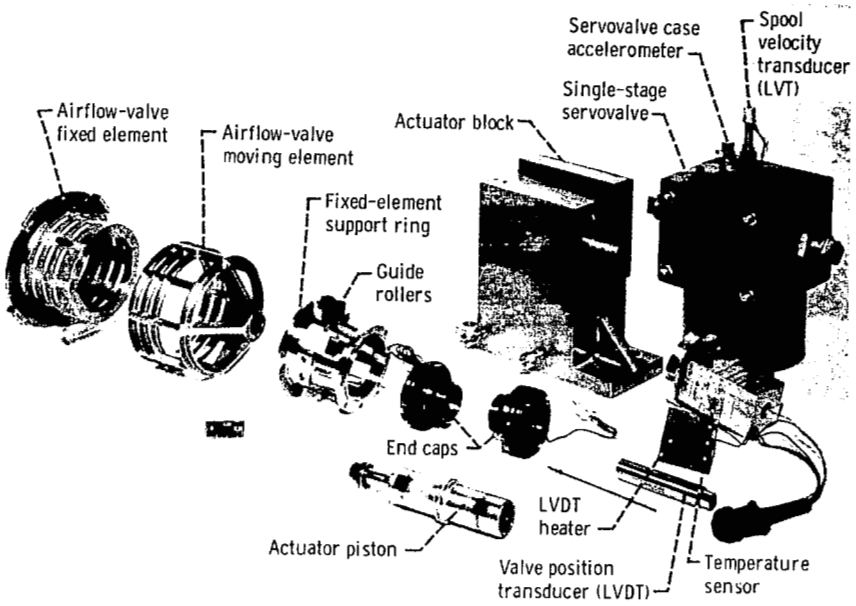

(a) Overall.

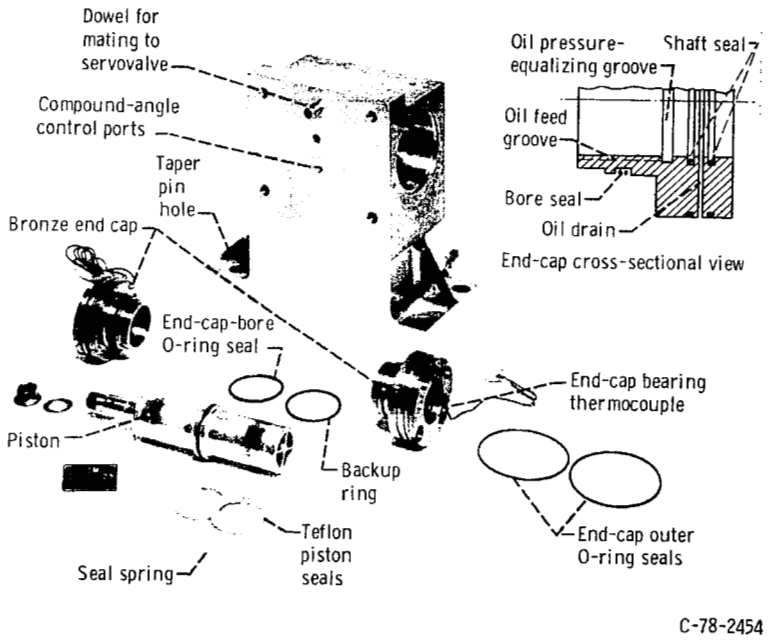

(b) Actuator block.

Figure 5. - Airflow-valve servosystem - disassembled views.

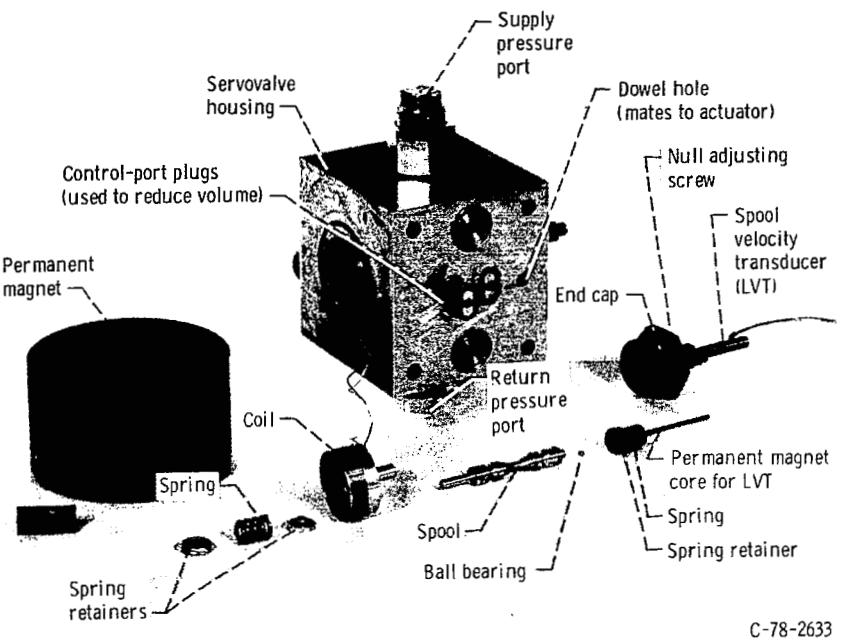

(c) Single-stage servovalve.

Figure 5. - Concluded.

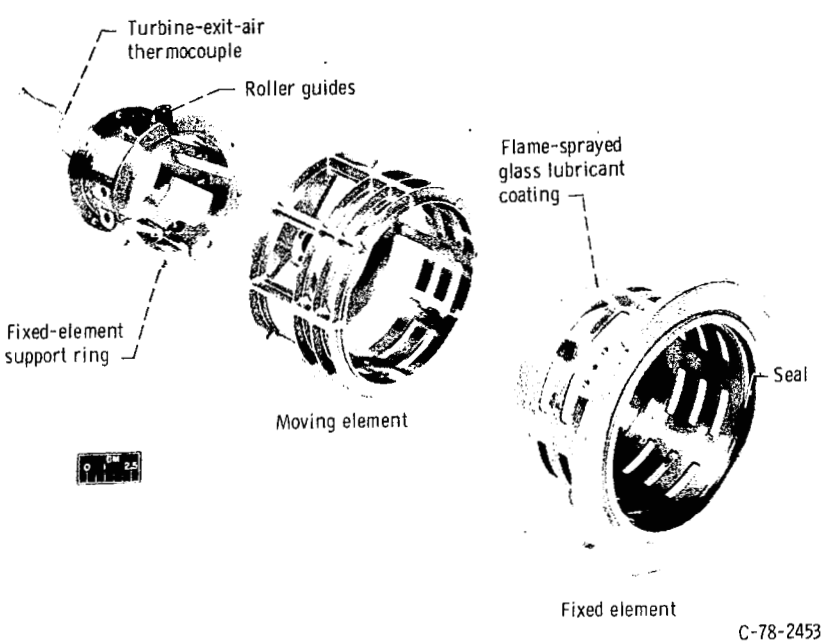

Figure 6. - Airflow-valve moving and fixed elements.

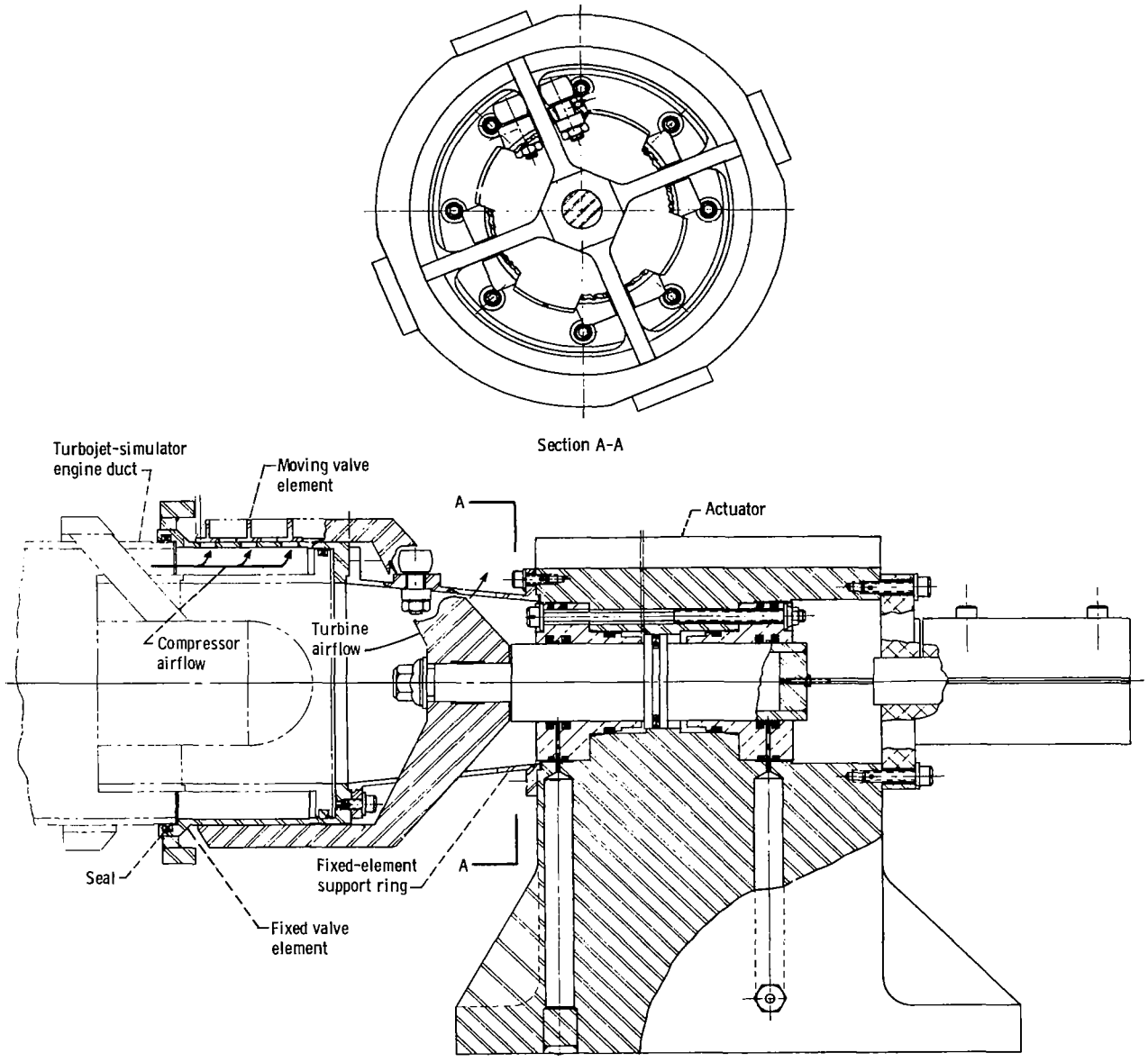

Figure 7. - Actuator and airflow-valve assembly. (Valve shown in closed position.)

A plasma-sprayed metal-glass-fluoride lubricant coating (NASA PS101) was successfully used. The coating was applied 0.254-millimeter (0.010-in.) thick and was machined to a surface finish of 0.81 micrometer rms (32-μin. rms) with a final thickness of approximately 0.127-millimeter (0.005-in.). To prevent smearing of the lubricant surface during machining, a single-point carbide tool and 0.051-millimeter (0.002-in.) long (or less) cuts were used. Further details regarding the coating material can be obtained from references 13 and 14.

Materials.—Nonmagnetic materials were used in both the fixed and moving elements of the valve to prevent contamination from metal particles. Contamination would be likely to occur with magnetic materials because of the magnetic field from the servovalve permanent magnet. The other factors influencing material choice for the valve

moving element were the maximum airflow temperature of 422 K (300° F) through the valve, the need for high stiffness and strength to avoid resonance and fatigue problems, and the need for a small moving-element mass. The final choice of material was 304 stainless steel for the fixed element and A286 stainless steel for the moving element.

Structural dynamics.—The major design goals for the valve moving element were minimum mass, high natural frequencies, adequate strength for dynamic and pressure loads, and minimum deflections during high-frequency oscillations. A NASTRAN structural static- and normal-mode analysis was performed for the valve moving element. A model showing the NASTRAN elements is given in figure 8. By using an iterative design process, individual parts of the structure were modified according to a previous analysis until the four major design objectives were satisfied. In the final design the first normal mode was a torsional displacement about the valve translational centerline at 668 hertz. The second normal mode was a lateral displacement at 929 hertz in a direction perpendicular to the valve translational axis. These frequencies are sufficiently above the operating frequencies of the servosystem to be considered acceptable. Plots of the NASTRAN graphic output for these modes are shown in figure 9.

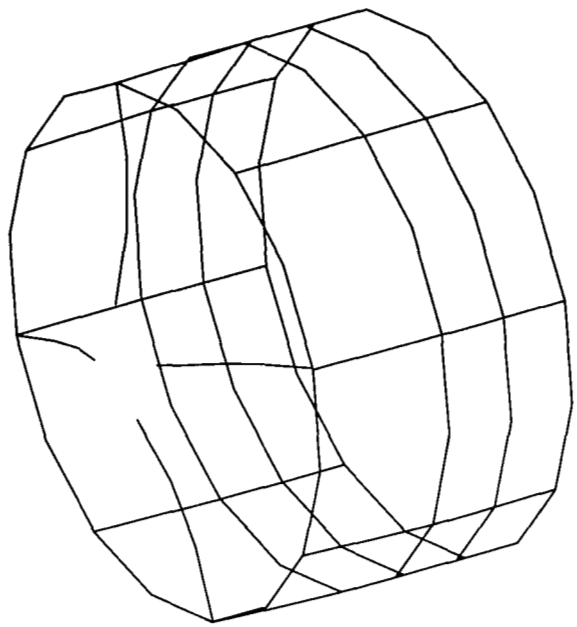

Figure 8. - Airflow-valve NASTRAN model - undeformed shape.

Servosystem Analysis

A nonlinear dynamic model of the airflow-valve servosystem that was programmed on an analog computer is described. In addition, a brief description of a nonlinear performance-limit criterion is provided. The model was used to select compensation techniques, to size components, and to set gains for the control system in the design stage. Once the model had been verified, it became a very useful tool for analyzing stabilization control techniques as well.

Derivation of Model

A block diagram of the system is shown in figure 10. The basic elements of the diagram are the electronic controller, the power amplifier and servovalve coil, the servovalve-spool dynamics, the servovalve orifices, and the actuator piston and load.

Controller.—The controller for the airflow-valve servosystem was an analog device consisting of operational amplifiers used for summing and compensating the feedback and command signals. The precompensator consisted of two parts: a second-order, lead-lag compensator; and a slew-rate limiter. The transfer function for the lead-lag compensator is given by

$$\frac{e_{cc}}{e_{com}} = \frac{s^2/\omega_1^2 + 2\zeta_1 s/\omega_1 + 1}{s^2/\omega_2^2 + 2\zeta_2 s/\omega_2 + 1} \tag{1}$$

The symbols used for this analysis are defined in appendix A. The slew-rate limiter was used to limit the velocity of the commanded airflow-valve position signal. The signal was formed by generating an approximate signal derivative, limiting it, and integrating the result. The derivative was formed as the difference between the input and the output:

$$\dot{e}_{pre} = (e_{cc} - e_{pre})/\text{sec} \tag{2}$$

This difference was limited in magnitude and integrated to form the velocity limiter output

$$e_{pre} = \int (\dot{e}_{pre})_{lim}\, dt \tag{3}$$

The controller then subtracted the valve-position feedback signal from the output of the precompensator and applied a forward-loop gain K_e.

$$K_e e_e = K_e(e_{sel} - e_{pre} - K_{vl} x_v) \tag{4}$$

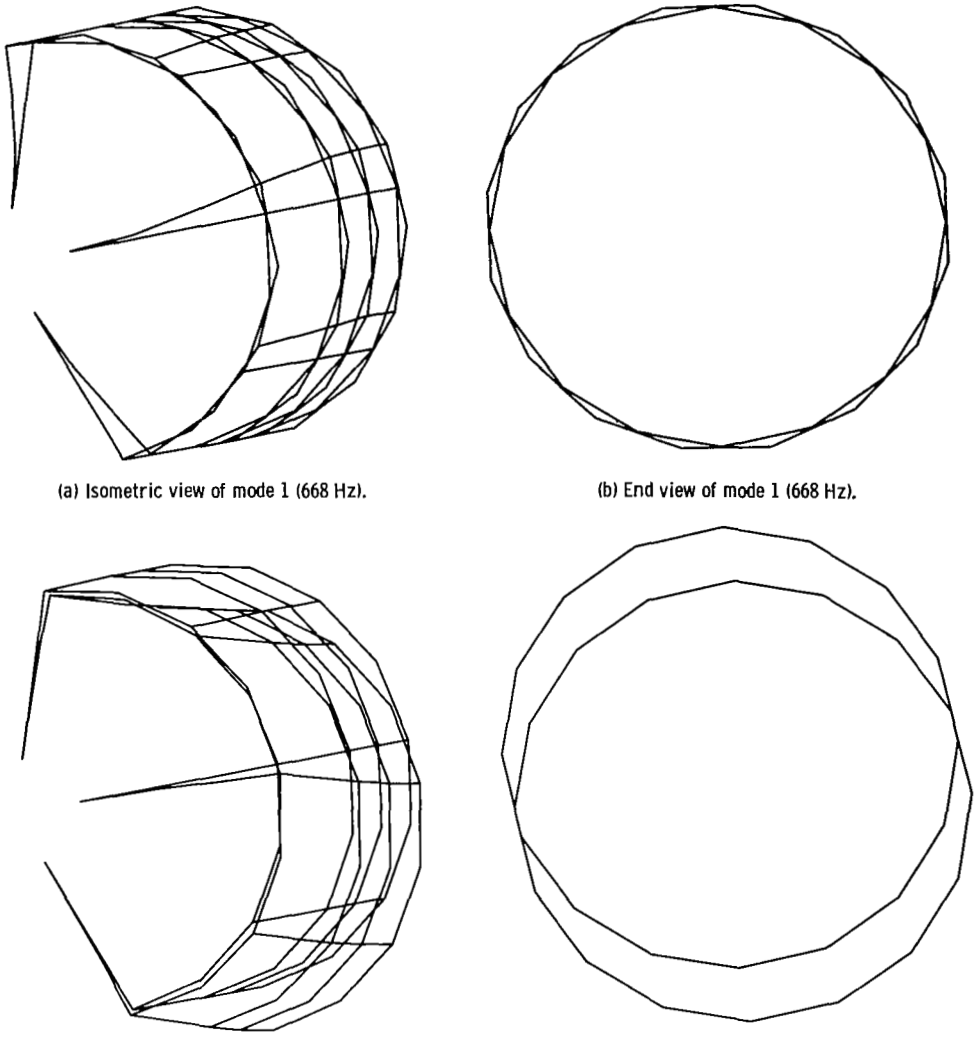

(a) Isometric view of mode 1 (668 Hz).

(b) End view of mode 1 (668 Hz).

(c) Isometric view of mode 2 (929 Hz).

(d) End view of mode 2 (929 Hz).

Figure 9. - Airflow-valve NASTRAN model - modal deformation.

This error signal was fed to a summing junction at the input of the power amplifier, where it was combined with the spool-velocity and coil-current feedback signals. The spool-velocity feedback compensator circuits were contained in the controller. This compensation consisted of a proportional gain term plus a high-pass-filtered integral term. The transfer function for this compensator was

$$\frac{e_s(s)}{\dot{x}_s(s)} = K_{sl}\left[K_{ps} + \frac{K_{is}\tau_1 s}{100(\tau_1 s+1)(\tau_2 s+1)}\right] \qquad (5)$$

The output e_s was fed to the input summing junction of the power amplifier.

Power amplifier and servovalve coil.—The input summing junction of the power amplifier was used for differencing the position error signal with the spool-velocity and coil-current feedback signals, as shown in figure 11. The equation describing this summation was

$$e_{pa} = \left[K_{pa}\left(\frac{1}{R_8}K_e e_e - \frac{1}{R_6}\,e_i - \frac{1}{R_9}e_s\right)\right]_{lim} \qquad (6)$$

where $K_e e_e$ and e_i were supplied by the controller. The power-amplifier output voltage saturation at

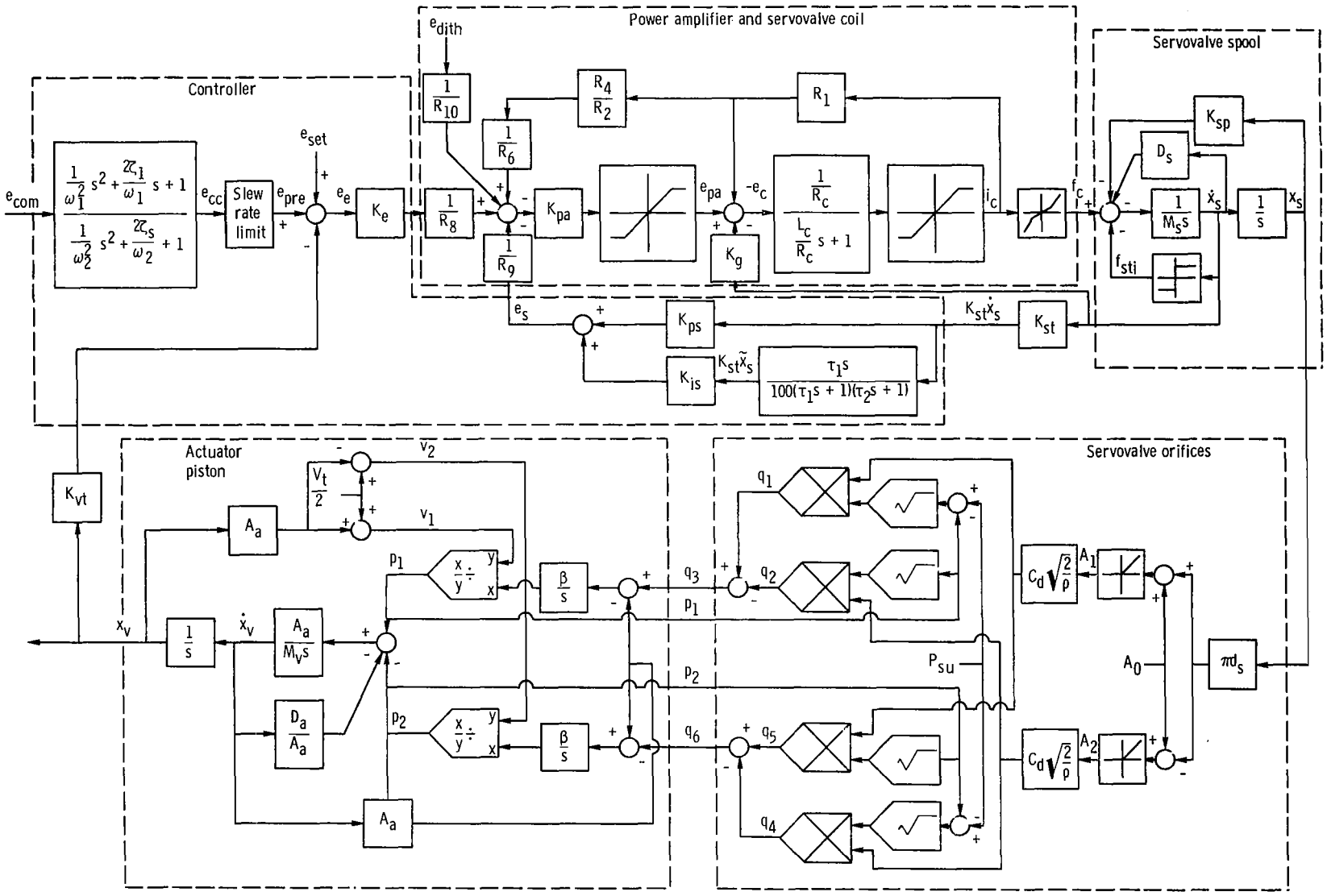

Figure 10. - Block diagram of airflow-valve servosystem model.

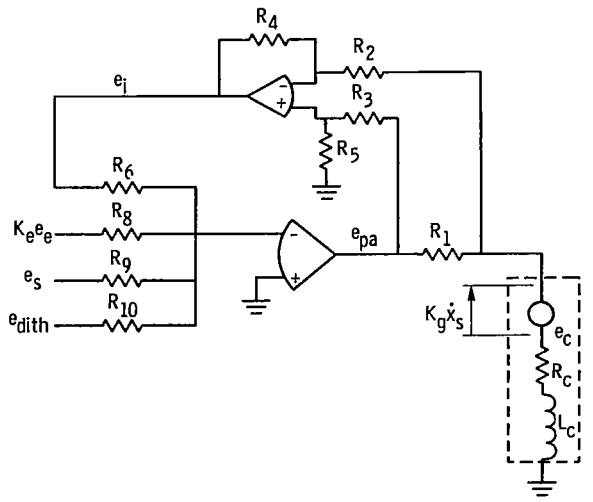

Figure 11. - Schematic of power amplifier and servovalve coil.

about 35 volts is modeled in figure 10 with a limiter on e_{pa}. A voltage signal proportional to coil current was formed by measuring the voltage drop across the series resistor R_1. This signal was measured with a differential operational amplifier with gain to produce e_i; thus

$$e_i = \frac{R_4}{R_2} R_1 i_c \tag{7}$$

The voltage applied to the servovalve coil was formed by subtracting the drop across R_1 and the back electromotive force of the coil from e_{pa}.

$$e_c = e_{pa} - R_1 i_c - K_g \dot{x}_s \tag{8}$$

The servovalve coil was modeled as a first-order lag formed by the resistance-inductance of the coil.

$$i_c(s) = \left[\left(\frac{1/R_c}{sL_c/R_c + 1} \right) e_c(s) \right]_{lim} \tag{9}$$

The output current of the power amplifier was limited at 6.2 amperes to protect the coil from thermal damage. The mechanical force that the coil applied to the spool was a nonlinear function of the coil current ($f_c = F(i_c)$). Figure 12 shows the steady-state plot of spool position versus coil current measured experimentally. This curve was obtained with the hydraulic system pressurized, but with no flow through the servovalve orifices. Flow forces on the spool were assumed to be balanced. The coil force being applied could be determined by multiplying the values on the x-axis by the spring rate K_{sp}. the force was linear with coil current for currents beyond 1.5 amperes, and the gain of f_c/i_c decreased near zero current or valve null. This function was modeled with a piecewise linear equation:

$$f_c = S_2 i_c - (S_2 - S_1)(i_c)_{lim,1.5\ amperes} \tag{10}$$

where S_1 is the slope of the force-current curve at null and S_2 is the slope of the curve for currents beyond 1.5 amperes.

Servovalve-spool dynamics.—The spring-mass dynamics of the servovalve spool were modeled by a second-order, linear transfer function formed by summing forces acting on the spool. This resulted in

$$\frac{x_s(s)}{f_c(s)} = \frac{1/K_{sp}}{s^2 M_s/K_{sp} + sD_s/K_{sp} + 1} \tag{11}$$

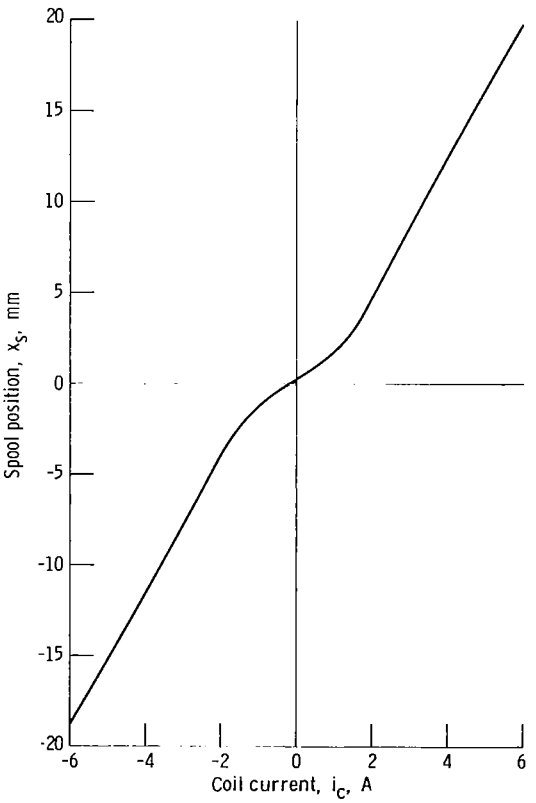

Figure 12. - Single-stage servovalve nonlinearity at null.

The spool motion exhibited stiction as well as viscous friction, and this required a dither signal to be summed at the power amplifier. Stiction was modeled for the analog computer by adding a stiction force level to the spool force summation that was constant and in a direction to oppose spool motion.

$$f_{sti} = -F_{sti}(sign\ \dot{x}_s) \tag{12}$$

Servovalve orifices.—The servovalve flowpaths consisted essentially of four orifices, as shown in figure 13. Because of symmetry, the orifices that passed q_1 and q_5 had essentially the same flow area as did orifices q_2 and q_4. The servovalve used for this system had an open center area A_0 created by valve underlap. Equations for valve areas can be written as

For $x_s > -x_{s,und}$

$$A_1 = A_5 = A_0 + \pi d_s x_s \tag{13}$$

$$A_2 = A_4 = 0 \tag{14}$$

For $x_s < +x_{s,und}$

$$A_1 = A_5 = 0 \tag{15}$$

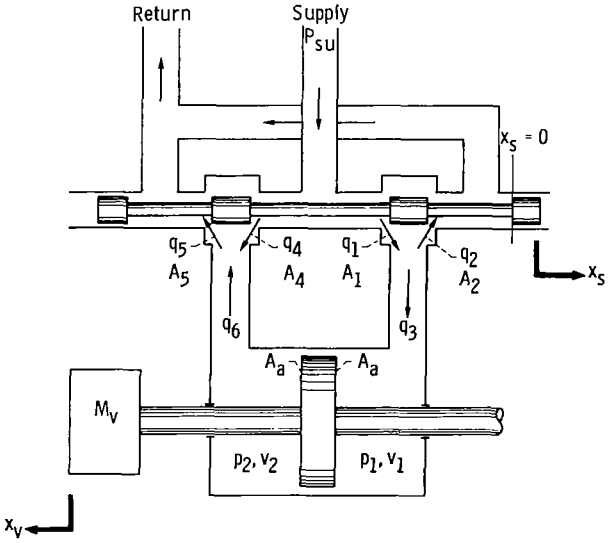

Figure 13. - Schematic of actuator hydraulic circuit.

$$A_2 = A_4 = A_0 - \pi d_s x_s \tag{16}$$

where

$$A_0 = \pi d_s x_{s,und} \tag{17}$$

The fluid flows through the orifices (ref. 15) are described by

$$q_1 = C_d A_1 \left[\frac{2}{\rho}(P_{su} - p_1)\right]^{1/2} \tag{18}$$

$$q_2 = C_d A_2 \left(\frac{2}{\rho} p_1\right)^{1/2} \tag{19}$$

$$q_4 = C_d A_4 \left[\frac{2}{\rho}(P_{su} - p_2)\right]^{1/2} \tag{20}$$

$$q_5 = C_d A_5 \left(\frac{2}{\rho} p_2\right)^{1/2} \tag{21}$$

It has been assumed that the return pressure at the servovalve was zero. The net flow in each control port of the servovalve was

$$q_3 = q_1 - q_2 \tag{22}$$

$$q_6 = q_5 - q_4 \tag{23}$$

Actuator piston and load.—The actuator consisted of two pressurized volumes acting on the piston area to accelerate the airflow-valve moving element (shown as M_v in fig. 13). The volumes were determined by adding or subtracting the amount of piston offset volume (from center) to or from one-half of the total fluid volume in the control ports and actuator.

$$v_1 = \frac{V_t}{2} + A_a x_v \tag{24}$$

$$v_2 = \frac{V_t}{2} - A_a x_v \tag{25}$$

The pressure in each volume was determined by writing continuity equations

$$p_1 = \frac{\beta}{v_1}\int(q_3 - A_a\dot{x}_v)dt \tag{26}$$

$$p_2 = \frac{\beta}{v_2}\int(A_a\dot{x}_v - q_6)dt \tag{27}$$

The load on the actuator was treated as an inertia load with some viscous damping, or

$$\dot{x}_v = \int\left[\frac{A_a}{M_v}(p_1 - p_2) - \frac{D_v}{M_v}\dot{x}_v\right]dt \tag{28}$$

These equations describe the airflow-valve servosystem model and provide the basis for the block diagram of figure 10. This model was programmed on an analog computer, which provided a real-time simulation of the airflow-valve servosystem. The analog computer model is described in appendix B. The values of the physical parameters used with this model are presented in table II.

TABLE II. – AIRFLOW-VALVE SERVOSYSTEM PARAMETERS

Controller:	
Precompensator lead frequency, ω_1, rad/sec	$2\pi(315)$
Precompensator lead damping ratio, ζ	0.50
Precompensator lag frequency, ω_2, rad/sec	$2\pi(950)$
Precompensator lag damping ratio, ζ	0.50
High-pass-filter time constant, τ_1, sec	0.02
Integrator low-frequency cutoff time constant, τ_2, sec	0.01
Error gain, K_e, V/V	1.70
Gain proportional to spool velocity, K_{ps}, V/V	5.04
Integral of spool velocity gain, K_{is}, sec^{-1}	1.313×10^4
Power amplifier and servovalve coil:	
Power amplifier resistors, Ω	
R_1	0.28
R_2	40 200
R_4	11 000
R_6	127
R_8	2000
R_9	2000
Power amplifier voltage-to-current gain, K_{pa}, V/A	25×10^3
Coil resistance, R_c, Ω	3.0
Coil inductance, L_c, H	1.0×10^{-3}
Average coil force-to-current gain, K_c, N/A	13.34
Servovalve spool dynamics:	
Spool mass, M_s, N sec^2/cm	1.124×10^{-3}
Spring rate, K_{sp}, N/cm	4404
Spool spring-mass system damping, D_s, N sec/cm	0.078
Servovalve orifices:	
Null flow-pressure coefficient, $K_{fp,0}$, cm^5/N sec	7.15×10^{-2}
Spool diameter, d_s, cm	1.316
Orifice discharge coefficient, C_d	0.6
Leakage orifice area at null, cm^2	1.548×10^{-2}
Hydraulic fluid:	
Hydraulic supply pressure, P_{su}, N/cm^2	2068
Density, ρ, N sec^2/cm^4	8.175×10^{-6}
Bulk modulus, β, N/cm^2	6.895×10^4
Actuator piston:	
Full stroke (zero to peak), cm	0.318
Area, A_a, cm^2	3.200
Total hydraulic-fluid volume in actuator, V_t, cm^3	28.68
Mass of piston and load-valve moving element, M_v, N sec^2/cm	1.122×10^{-2}
Damping factor, D_a, N sec/cm	1.016
Transducer gains:	
Load-valve position transducer, K_{vt}, V/cm	15.75
Servovalve-spool velocity transducer, K_{st}, V sec/cm	0.0472
Saturation levels:	
Coil-current saturation, $I_{c,sat}$, A	6.2
Coil-voltage saturation, $E_{pa,sat}$, V	35

Nonlinear Performance Limits

An electrohydraulic servosystem design is usually based on the linear dynamics of the system and optimization of the linear response (refs. 16 and 17). However, this system was limited in its dynamic performance by such nonlinearities as signal saturations or limited available hydraulic power. Such performance limits tend to degrade the dynamic performance of the servoactuator from its linear response for large-amplitude motions. These limits, modeled as straight lines on amplitude Bode plots, define an upper bound of performance.

The effect of such nonlinearities on the performance of servosystems using two-stage electrohydraulic servovalves is analyzed in reference 10. That analysis derived acceleration and flow limits on the dynamic response of the hydraulic actuator servosystem. The acceleration limit can be directly applied to this system design, but the flow through the single-stage servovalve is limited by different phenomena. The maximum flow of the single-stage servovalve is set by the maximum spool displacement achieved when applying full electrical power to the spool coil driver. Therefore the flow is limited by the coil-current and voltage saturation levels of the power amplifier driving the coils. Reference 18 presents a derivation of the acceleration, coil-current, and coil-voltage limit lines for the airflow-valve servosystem. The acceleration limit line is defined by the maximum-load mass acceleration

TABLE III. - SUMMARY OF AIRFLOW-VALVE LIMIT-LINE EQUATIONS

Limit line	Equation	Value
Acceleration limit	$\lvert X_v \rvert \omega^2 = \frac{2\sqrt{2} A_a P_{su}}{3M_v}$	5.561×10^5 cm/sec^2
Coil-current limit at low frequency[a]	$\lvert X_v \rvert \omega = \frac{4K_f K_c I_{c,sat}}{\pi K_{sp} A_a}$	2.407×10^2 cm/sec
Coil-current limit at high frequency[a]	$\lvert X_v \rvert \omega^3 = \frac{4K_f K_c I_{c,sat}}{\pi M_s A_a}$	9.430×10^8 cm/sec^3
Coil-voltage limit at low frequency[a]	$\lvert X_v \rvert \omega = \frac{4K_f K_c E_{pa,sat}}{\pi K_{sp}(R_c + R_1) A_a}$	4.142×10^2 cm/sec
Coil-voltage limit at high frequency[a]	$\lvert X_v \rvert \omega^4 = \frac{4K_f K_c E_{pa,sat}}{\pi M_s L_c A_a}$	5.324×10^{12} cm/sec^4

[a] Where $K_f = \pi d_s C_d \left(\frac{2P_{su}}{3\rho}\right)^{1/2} = 3.221 \times 10^4$ cm^2/sec.

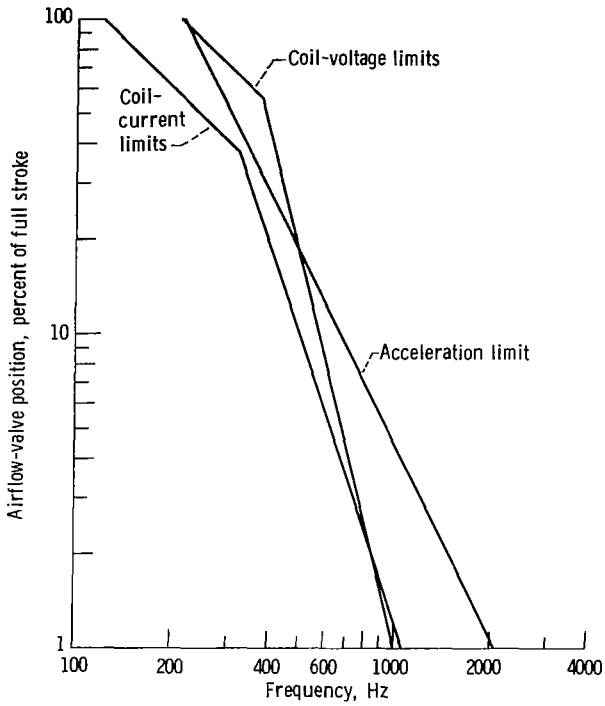

Figure 14. - Limit lines for predicting dynamic performance of airflow-valve servosystem. (Full stroke, 0.635 cm.)

obtainable for a given supply pressure P_{su} and piston area A_a. The coil-current and coil-voltage limits were derived as asymptotic straight-line approximations to the low- and high-frequency dynamic limitations of system performance on the basis of saturation levels. The limit-line equations are summarized in table III, and the lines are plotted on the amplitude Bode plot in figure 14. The most restrictive of these lines (lowest frequency and amplitude) predicts the maximum dynamic performance achievable for the servosystem amplitude response.

The servovalve and power amplifier used were commercially available designs; thus the values for d_s, K_c, K_{sp}, M_s, R_c, R_1, L_c, $E_{pa,sat}$, and $I_{c,sat}$ were fixed. The hydraulic supply pressure P_{su} and fluid density ρ were also set by the available equipment. The minimum moving-element mass M_v was determined from structural design considerations. Therefore the only parameter available to adjust the position of the limit lines was actuator-piston area A_a.

The magnitude of the acceleration limit line is a direct function of piston area; the coil-current and coil-voltage limits vary inversely with piston area. The movement of a typical set of coil-current and acceleration limit lines for decreasing piston area is shown in figure 15. The coil-current lines move toward increasing amplitudes and frequencies; the acceleration limit line moves toward decreasing amplitudes and frequencies. To select a piston area

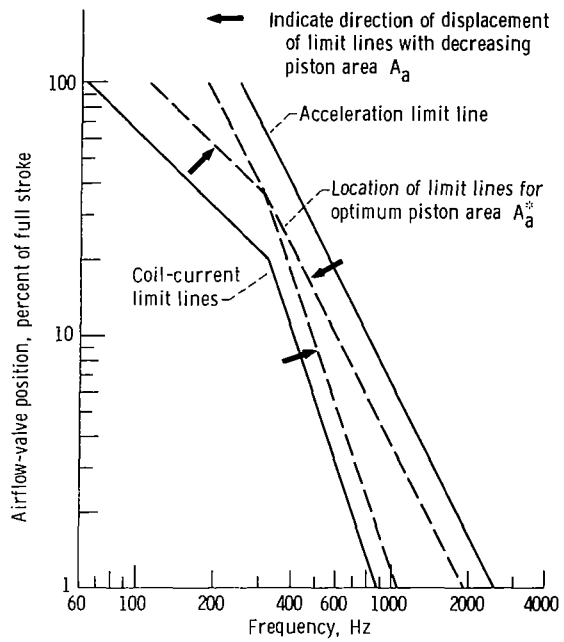

Figure 15. - Effect of actuator-piston area on limit-line locations. (Full stroke, 0.635 cm.)

that would tend to maximize the system response, the point where the low- and high-frequency current limit lines intersect each other was equated to the acceleration limit line.

$$A_a^* = \left[\frac{3\sqrt{2} K_l K_c I_{c,sat} M_v}{\pi P_{su} (M_s K_{sp})^{1/2}} \right]^{1/2} \tag{29}$$

The actuator area that will make the limit lines intersect A_a is shown by the dashed lines in figure 15. From the parameters in table II the optimum area is 2.96 square centimeters. The actual area used was 3.20 square centimeters, which was a design compromise based on piston-seal sizing considerations. A larger-than-optimum area was used because this made coil current the predominant limit. Since the dynamics downstream of the current saturation contained a lightly damped resonance, the actual system response probably exceeded the coil-current limit line near the resonance. The resulting limit lines for an area of 3.20 square centimeters are plotted in figure 14.

The presence of lightly damped poles downstream of the saturating device requires that the limit lines be solved for more exactly by using transfer-function magnitudes instead of asymptotes. Besides the resonance of the servovalve-spool spring mass, there exists a second-order resonance formed by the stiffness of the hydraulic fluid driving the piston mass M_v. The limit line for coil-current saturation derived in reference 18 is

$$|x_v|_\omega = \frac{4 K_l K_c I_{c,sat} / \pi K_{sp} A_a}{\left| \left[1 - \left(\frac{\omega}{\omega_{ns}} \right)^2 \right] + j 2 \zeta_s \left(\frac{\omega}{\omega_{ns}} \right) \right| \left| \left[1 - \left(\frac{\omega}{\omega_{nh}} \right)^2 \right] + j 2 \zeta_h \left(\frac{\omega}{\omega_{nh}} \right) \right|} \tag{30}$$

which is the equation for the complex coil-current limit line, where

$$\omega_{ns} = \left(\frac{K_{sp}}{M_s} \right)^{1/2} \tag{31}$$

$$\zeta_s = \frac{D_s}{2 (K_{sp} M_s)^{1/2}} \tag{32}$$

$$\omega_{nh} = 2 A_a \left(\frac{\beta}{V_t M_v} \right)^{1/2} \tag{33}$$

$$\zeta_h = \frac{K_{fp0}}{2 A_a} \left(\frac{2 \beta M_v}{V_t} \right)^{1/2} \tag{34}$$

This limit line for the airflow-valve servosystem is plotted on the data presented in the results section for comparison with the actual system response.

Dynamic Performance of Servosystem and Model

Test Procedures

Dynamic data were obtained by applying a sinusoidal command signal to the controller for various amplitude levels and sweeping the frequency of this signal from 10 to 1000 hertz. Data were recorded on an analog, 14-channel FM tape recorder and analyzed with a frequency-response analyzer that provided amplitude and phase plots as functions of frequency. Step-response data were also recorded.

The airflow-valve actuator was mounted to a T-slot bedplate on the floor of the test cell for initial response testing of the servosystem (fig. 1). these tests provided for checking the piston structural vibration amplitudes with a dummy mass load, for evaluating end-cap impact protection, and for adjusting compensation circuits and system gains. The design development during preliminary testing is discussed in appendix C. Once satisfactory performance was obtained with the dummy mass, the airflow valve was assembled on the actuator to evaluate its function with dynamic excitation. When the airflow valve was used in compressor studies, the servosystem had to be mounted on a nonrigid structure (fig. 3). Again data were taken and the acceleration feedback scheme described in appendix C was implemented. All the data presented in this section were taken with the actuator mounted on the test stand and the acceleration feedback employed.

System Transfer-Function Results

Dynamic data were used to verify the model as well as to determine the experimental performance of the position servosystem. These data helped to determine

parameters that could not easily be measured by other means. The transfer functions for forward-loop dynamics are presented here for an excitation amplitude of 10 percent of full scale. This low level was chosen to minimize the effect on the data of the nonlinear-element saturation levels (fig. 10).

Servovalve-coil dynamics.—The Bode plot of the servovalve-coil dynamics, or the response of coil-current to power-amplifier output voltage i_c/e_{pa}, is presented in figure 16. According to the block diagram of figure 10, these data should show the first-order lag with a time constant of $L_c/(R_c+R_1)$ (0.3 msec, or a corner frequency of 520 Hz). The amplitude dynamics of figure 16(a) show a lower response than does the model. However, the phase-angle results (fig. 16(b)) remain relatively flat at high frequencies. The large notch in the amplitude plot at 315 hertz was a result of the back electromotive force generated on the coil as the servovalve passed through the spring-mass resonance of the spool. This additional feedback loop (see K_g in fig. 10) can be viewed as a second-order lag (with rate) in the feedback path that will create a notch when lightly damped. The match with the model is not critical at this level since the overall dynamics of the coil-current loop are determined by the coil-current feedback gain.

Closed-loop response of coil-current loop.—The response of the coil current (measured as e_i) to the net input at the power amplifier $K_e e_e - e_s$ is shown in figure 17. The current feedback has increased the current response to the equivalent of a first-order lag with a corner frequency of about 1000 hertz. This feedback has also minimized the effect of the coil back electromotive force on the current response.

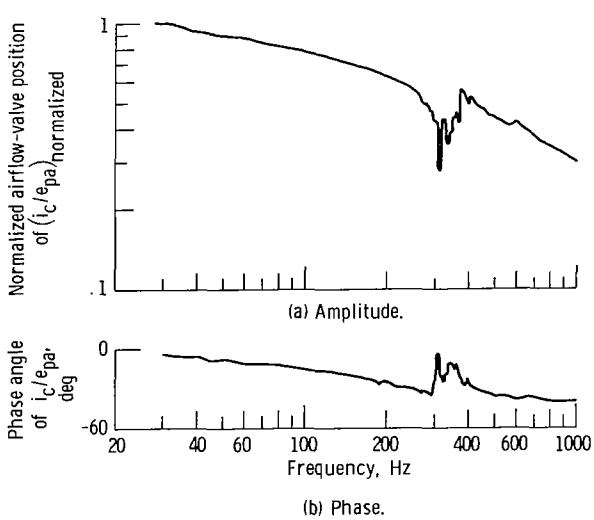

Figure 16. - Servovalve-coil dynamics - frequency response. Airflow-valve position, 10 percent of full stroke. Full stroke, 0.635 cm.

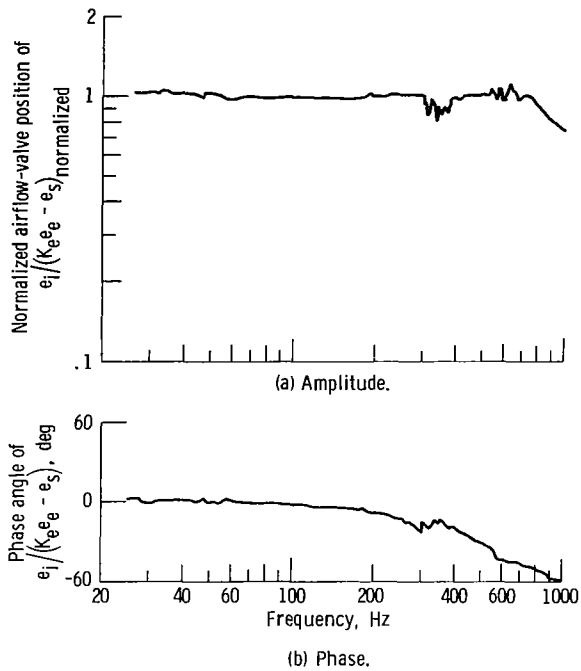

Figure 17. - Coil current - closed-loop frequency response. Airflow-valve position, 10 percent of full stroke. Full stroke, 0.635 cm.

Servovalve-spool spring-mass dynamics.—The frequency response of the servovalve-spool position $\tilde{x}_s$ relative to the coil current i_c is presented in figure 18 to determine the spring-mass resonant frequency and damping. The amplitude plot (fig. 18(a)) appears to decrease at low frequencies because the signal being used for x_s is obtained from the high-pass-filtered and integrated spool-velocity signal (similar to $K_{sl}\tilde{x}_s$ in fig. 10.) The resonant peak agrees well with the value obtained from $(K_{sp}/M_s)^{1/2}$, or 315 hertz. This also agrees with the 90° phase lag point of figure 18(b). Damping was very light, and the damping ratio was taken to be about 0.02 for the model. The effect of the structural mount vibration is seen at about 200 hertz.

Servovalve closed-loop spool dynamics.—The response of the servovalve-spool position $\tilde{x}_s$ relative to the actuator position error $K_e e_e$ is presented in figure 19. This transfer function defines the operation of the spool with the velocity loop closed. As shown in figure 19(a) the resonant frequency has been extended beyond the 315 hertz of the spring mass (to about 460 Hz), and damping has been increased to a damping ratio of 0.20. The phase plot (fig. 19(b)) shows that the 90° lag point occurred at about 460 hertz. The result is somewhat obscured by the occurrence of saturation near 600 hertz.

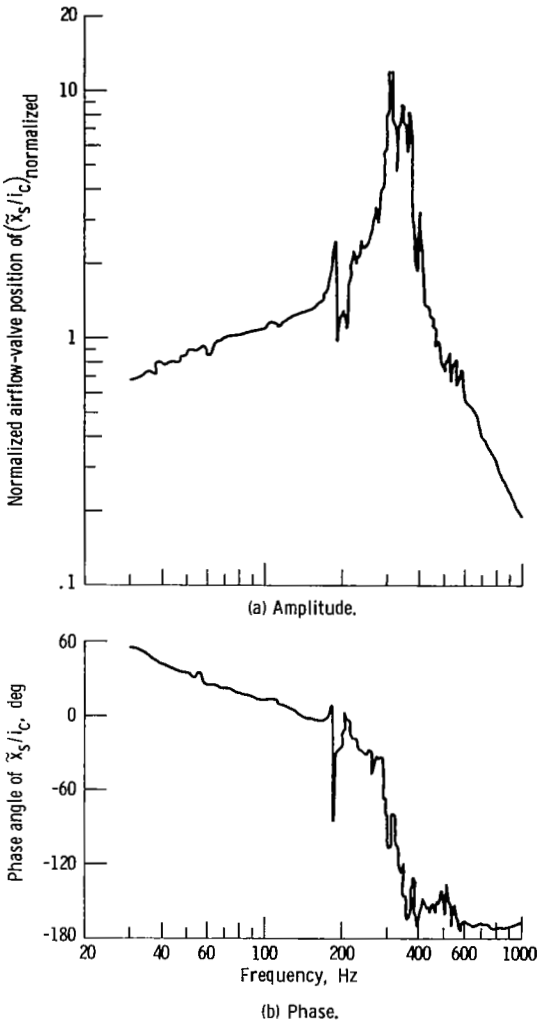

Figure 18. - Servovalve-spool position - open-loop frequency response. Airflow-valve position, 10 percent of full stroke. Full stroke, 0.635 cm.

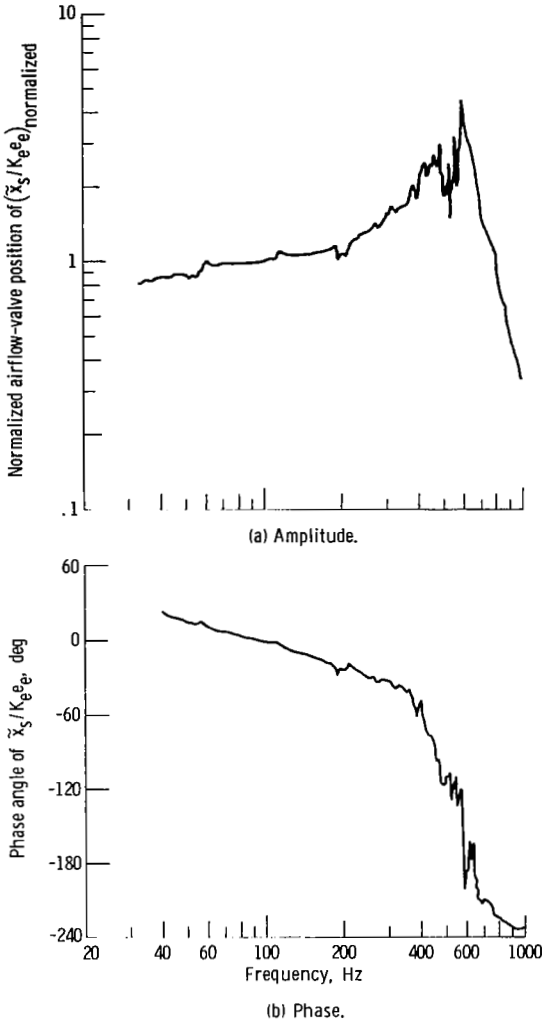

Figure 19. - Servovalve-spool position - closed-loop frequency response. Airflow-valve position, 10 percent of full stroke. Full stroke, 0.635 cm.

Actuator hydraulic-circuit dynamics.—The dynamics between the servovalve-spool position $\tilde{x}_s$ and the airflow valve position x_v are identified in figure 20. These dynamics include the second-order hydraulic resonant system created by the hydraulic spring rate and the piston load mass as well as the piston integration of flow. Figure 20(a) shows that the amplitude dropped off on a first-order slope until the resonance raised the amplitude. On the phase curve of figure 20(b), the integrator should have a phase lag of 90° at low frequencies. However, the actual signal used to generate spool position was high pass filtered, and this added phase at low frequency. The model gave a hydraulic resonant frequency of 472 hertz (eq. (33)), which should correspond to the 180° point on the phase curve. The phase at 472 hertz had about 18° more lag than expected. This may be due to dynamics that were not modeled, such as control-port flow lags.

Overall Dynamic Response of Airflow-Valve Servosystem

The response of airflow-valve position to a command input sine wave is presented in figure 21 for excitation amplitudes of 10, 20, 40, and 80 percent of full stroke (full stroke, 0.635 cm). The acceleration and complex coil-current saturation limit lines are also plotted on the amplitude curve in figure 21(a). The forward-loop gain was set

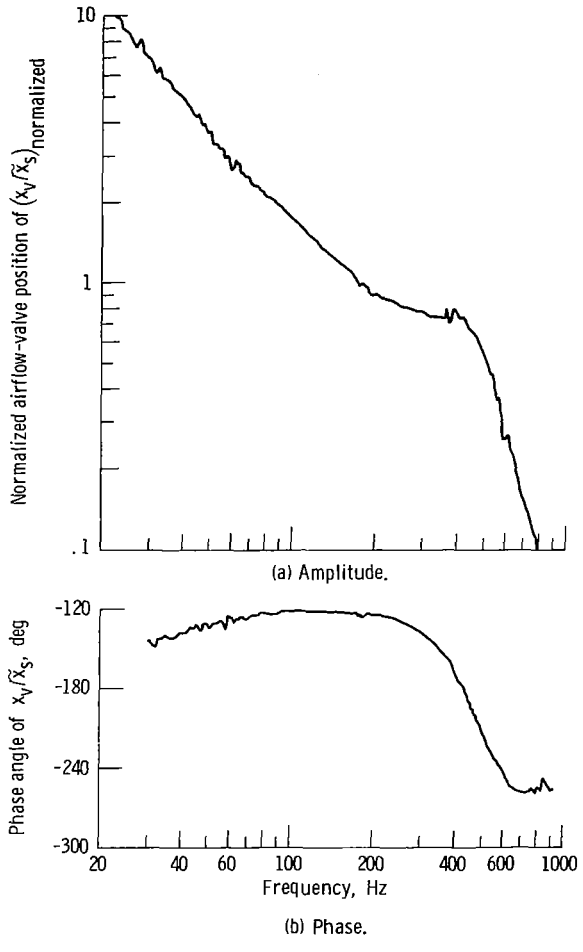

Figure 20. - Actuator hydraulic circuit - frequency response. Airflow-valve position, 10 percent of full stroke. Full stroke, 0.635 cm.

somewhat high, and this resulted in a lightly damped response at 10 percent of full stroke. However, when the excitation amplitude was increased, the nonlinear limits tended to clip the resonant amplitude peak and thus provided an effective increase in damping for large amplitudes. The 10 percent amplitude response was down 3 decibels at 640 hertz. Increasing amplitude decreased response and resulted in 3-decibel points of 490, 380, and 190 hertz for amplitudes of 20, 40, and 80 percent of full stroke, respectively. The degradation of response at 80 percent amplitude was caused by the velocity-limiting device in the precompensator. The somewhat erratic behavior between 500 and 600 hertz was related to the stiction levels in the spool valve interacting with the occurrence of current saturation. This interaction was eliminated in later runs by decreasing the dither frequency and increasing the dither signal amplitude at the power amplifier.

The phase curves in figure 21(b) show the effect of various amplitudes on phase response. An interesting result is that the phase response between 100 and 250 hertz shows more phase lag for the 10 percent amplitude excitation than for 40 percent. The system should be operating linearly and the phase curves should be identical. The nonlinearity responsible for this result is the low gain of the servovalve coil-current-to-coil-force function at null (fig. 10). When the system was operating at smaller amplitudes, this gain was small and thus the linear dynamics

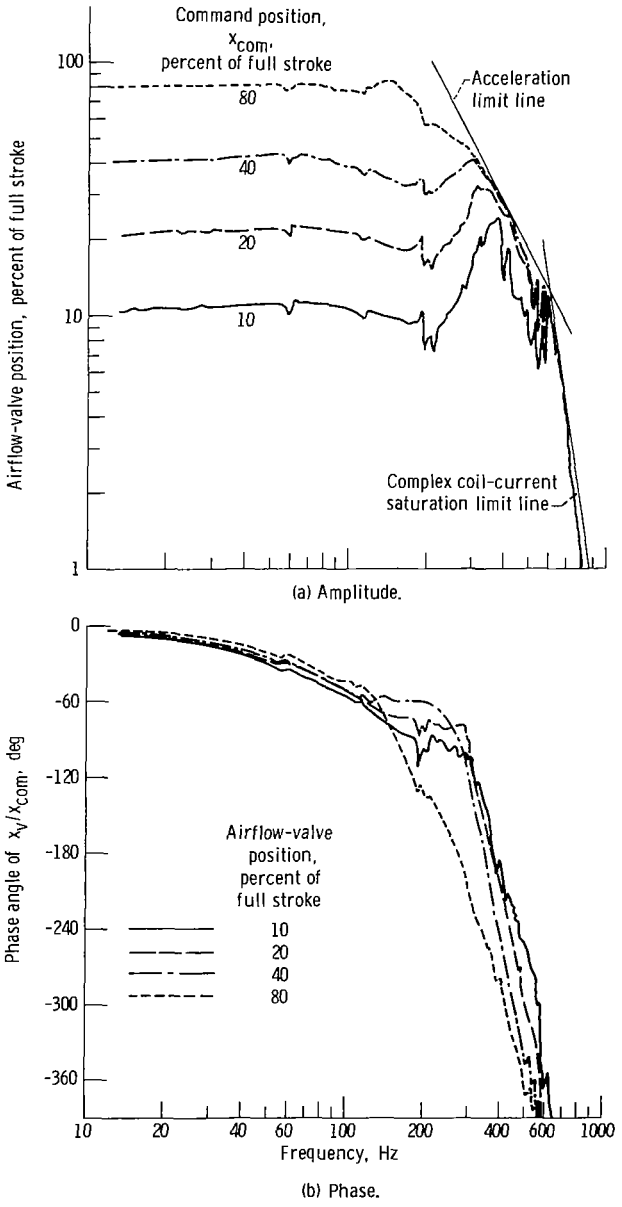

Figure 21. - Airflow-valve servosystem - closed-loop frequency response. Full stroke, 0.635 cm.

decreased. When the amplitude increased, the error signal (and the coil-current signal) increased and moved to the higher portion of the curve in figure 12. This higher gain tightened the overall control loop and provided the improvement in phase with larger amplitudes shown in figure 21(b). The specification given in table I that phase not exceed -90° at 200 hertz was met by this system, with the exception of the 80 percent amplitude curve, which was velocity limited.

Comparison of Results with Analog Computer Model

The overall response plots of figure 21 are compared with the results obtained with the analog computer model described in appendix B in figures 22 to 25 for excitation amplitudes of 10, 20, 40 and

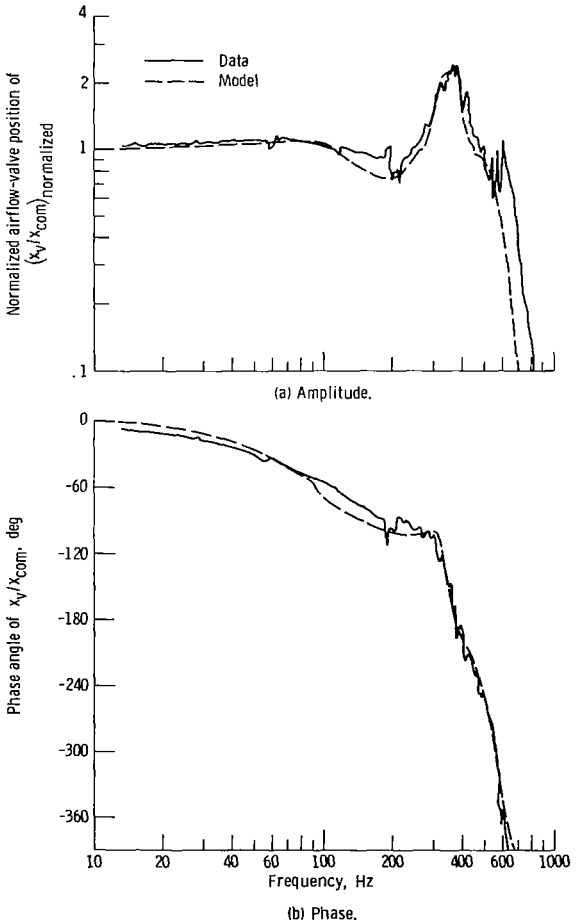

Figure 22. - Comparison of airflow-valve servosystem response with analog computer model at 10-percent-of-full-stroke amplitude.

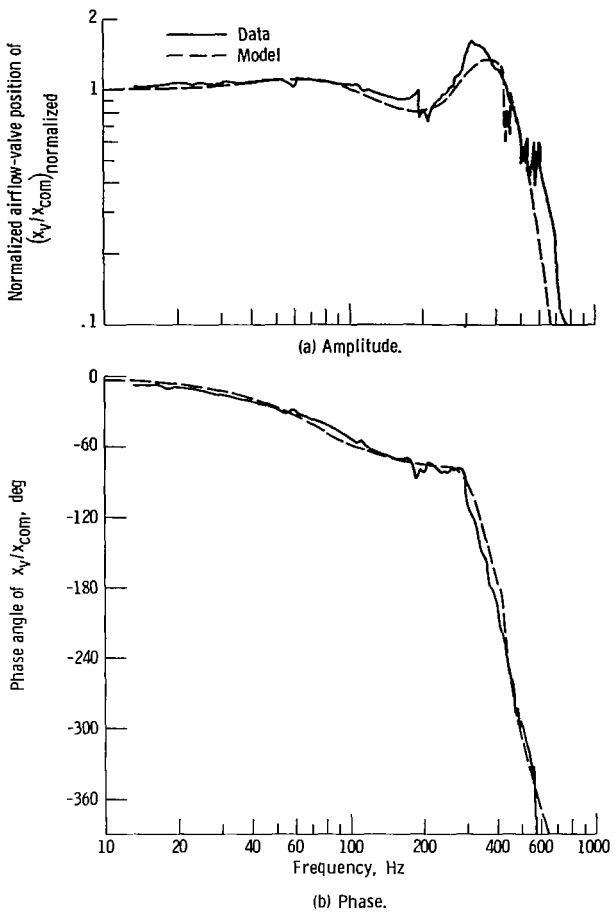

Figure 23. - Comparison of airflow-valve servosystem response with analog computer model at 20-percent-of-full-stroke amplitude.

80 percent of full stroke. Good agreement was obtained at all amplitudes although the location of the small-amplitude response for the model at high-frequency-limited operation (figs. 22 and 23) was below the results obtained experimentally. This was due in part to an adjustment of the coil-current limit to improve agreement with the phase response in parts (b) of these figures. The larger amplitude (40 and 80 percent of full stroke) responses shown in figures 24 and 25 were below the response of the system, and phase responses were slightly above. These results may be in error because the simulation may not include an adequate dynamic model of the hydraulic circuit. The 80 percent amplitude response for the model resulted from decreasing the velocity limit to improve phase agreement. Wherever possible the model was made more conservative than the actual system since it will be combined with a compressor model to predict preformance when used in various stabilizing control schemes. The amplitude

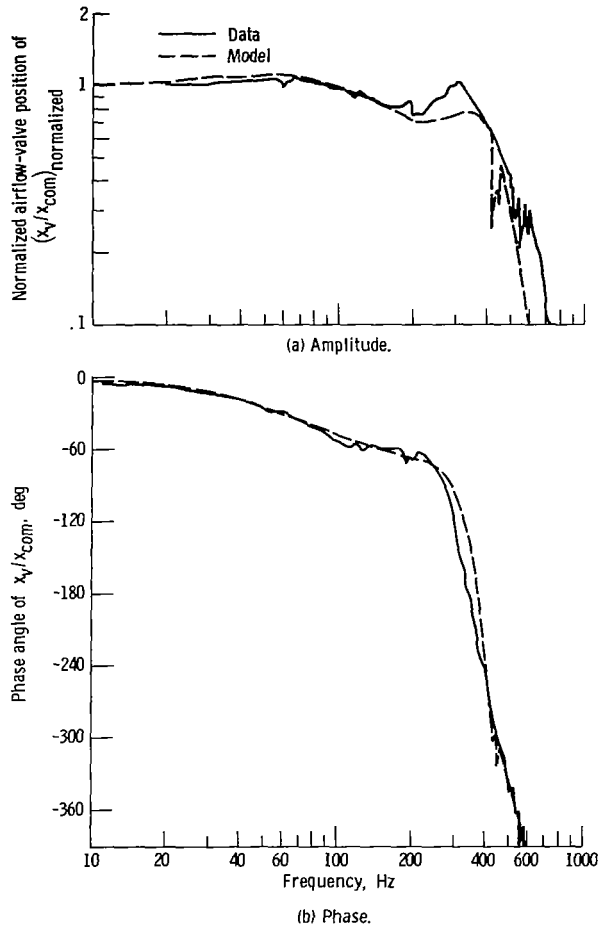

Figure 24. - Comparison of airflow-valve servosystem response with analog computer model at 40-percent-of-full-stroke amplitude.

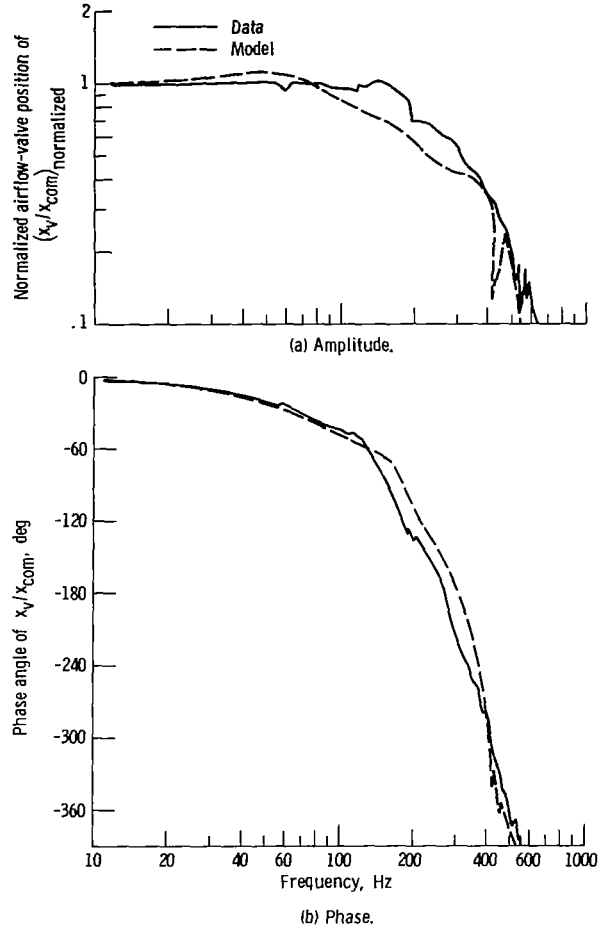

Figure 25. - Comparison of airflow-valve servosystem response with analog computer model at 80-percent-of-full-stroke amplitude.

plots of figures 22 to 25 demonstrate that the interaction of stiction with the coil-current saturation was also present in the model.

Airflow-Valve-Servosystem Step Response

A set of step responses for step sizes of 10, 20, 40 and 80 percent of full stroke is presented in figure 26. The airflow valve was stroked about its centered position. (The 80 percent amplitude step went from the 10 percent open to 90 percent open positions on the airflow valve.) The results show that the valve achieved full step amplitude in 2.8 milliseconds for the 10 percent amplitude step. The high order of this system created the apparent dead time at the beginning of the step response. The increase in damping for larger amplitudes caused by the nonlinearities is apparent in figures 26 (c) and (d) for the 40 and 80 percent amplitude steps.

Summary of Results

The design, analysis, and performance of an electrohydraulic servosystem for providing high-frequency positioning of an airflow valve have been presented. This system included the use of a single-stage electrohydraulic servovalve to obtain higher dynamic response capabilities than with conventional two-stage servovalves. The spring-mass resonance of the single-stage servovalve was very lightly damped and required velocity feedback for stabilization. Though lightly damped, the overall servosystem position response could be improved by adding a second-order lead-lag precompensator designed with frequency-domain techniques.

Using nonlinear limit criteria provided a useful technique for choosing actuator-piston area and predicting dynamic performance. However, when lightly damped resonances were present downstream

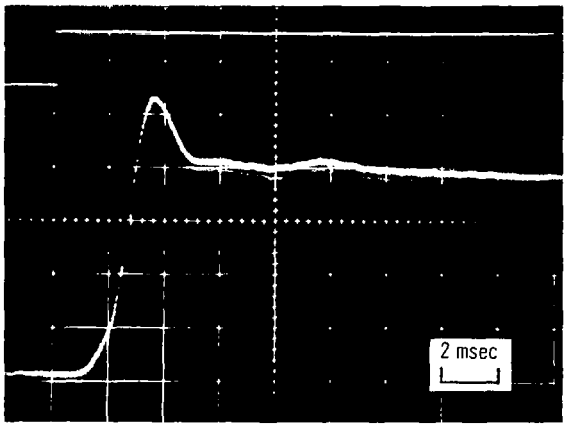

(a) 10-Percent-of-full-stroke step.

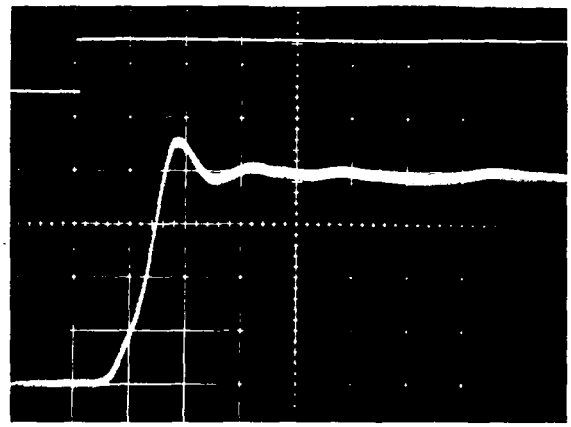

(b) 20-Percent-of-full-stroke step.

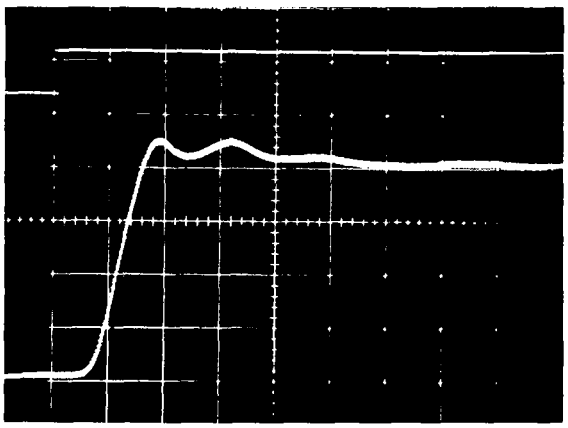

(c) 40-Percent-of-full-stroke step.

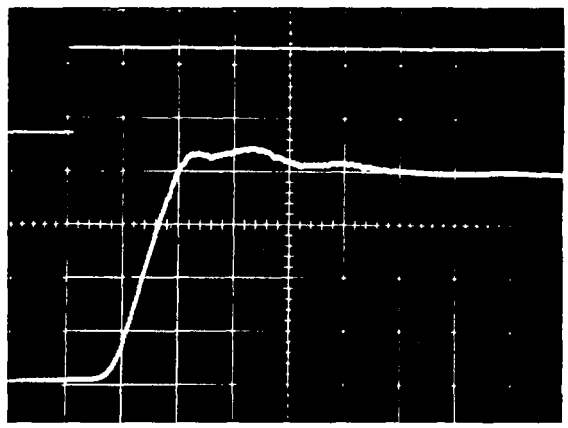

(d) 80-Percent-of-full-stroke step.

Figure 26. - Step response of airflow-valve servosystem for various amplitude steps.

of the element that was limiting, the system response could exceed the response predicted by the limit lines.

The airflow-valve moving element was designed with the aid of a NASTRAN structural static- and normal-mode analysis. The development of this servosystem pointed out the need to consider the structural modes of the actuator piston also since this design had a cantilevered load at one end of the piston.

Using a spring-centered spool valve with a large valve-area-to-spool-displacement gain created a potential stability problem when the servovalve case was subjected to vibration. Since a stiff mounting structure was not physically possible for this application, acceleration feedback was used to minimize the servovalve's vibration sensitivity.

The servosystem exhibited a dynamic response of -3 decibels at 490 hertz and a 90° phase lag at 300 hertz for excitation amplitudes of 20 percent of full stroke (where full stroke corresponds to 0.635 cm, or an airflow-valve area of 40 cm^2) with a 1.1-kilogram (2.5-lb) inertia load mass. The dynamic response of the servosystem degraded at larger amplitude excitations in accordance with the predicted limiting phenomena. The performance data were compared with analytical results obtained with an analog computer model. Good agreement was obtained for a wide range of excitation amplitudes.

Lewis Research Center,
National Aeronautics and Space Administration,
Cleveland, Ohio, January 8, 1980,
505-05.

Appendix A
Symbols

A	area, cm^2
C	orifice discharge coefficient
D	damping factor, N sec/cm
d	diameter, cm
e	airflow-valve servosystem voltage, V
F	force level, N
$F( )$	function of ( )
f	force signal, N
I	current level, A
i	current (time domain), A
K	gain
K_{ax}	airflow valve area-to-position gain, cm
K_c	linearized servovalve coil-force-to-coil-current gain, N/A
K_{fp0}	servovalve null flow-pressure coefficient, cm^5/N sec
K_l	linearized servovalve flow to maximum spool position for peak-power transfer point, cm^2/sec
K_{pa}	power-amplifier gain, V/A
K_{sp}	spring rate, N/cm
K_{st}	spool-velocity transducer gain, V sec/cm
K_{vt}	airflow-valve position transducer gain, V/cm
L	inductance, H
M	Mass, N sec^2/cm
P	pressure (steady state), N/cm^2
p	pressure (instantaneous), N/cm^2
q	volumetric flow (instantaneous), cm^3/sec
R	resistor, Ω
rms	root mean square
S	slope of coil-force-to-coil-current curve
s	Laplace operator
T	sine wave period, sec
t	time, sec
x	position, cm
V	volume (steady state), cm^3
v	volume (instananeous), cm^3
β	bulk modulus, N/cm^2
ρ	hydraulic-fluid density, N sec^2/cm^4
ζ	damping ratio
τ	time constant, sec
ω	frequency, rad/sec
$\lvert\ \rvert$	zero-to-peak amplitude of sinusoid

Subscripts:

a	actuator
ax	area to position
c	coil
cc	command compensator
com	command
d	discharge
dith	dither
e	error
fp0	flow to pressure at null
full	full stroke
g	back-electromotive-force generator
h	hydraulic
i	coil current
is	integral of spool velocity
l	linearized flow to maximum spool position
lim	limited signal
max	maximum
nh	hydraulic natural frequency
ns	spool natural frequency
pa	power amplifier
pre	precompensated command
ps	proportional to spool velocity
s	spool
sat	saturation
set	set point

sp	spring
st	spool-velocity transducer
sti	stiction
su	supply
t	total
und	underlap
v	airflow valve
vt	airflow-valve position transducer
0	null
1,2,...	numerical subscripts used as noted in text

Superscripts:

( )*	optimum
($\dot{}$)	first derivative with respect to time
($\tilde{}$)	high-pass-filtered signal

Appendix B

Analog Computer Model of Airflow-Valve Servosystem

The block diagram shown in figure 10 was implemented on an analog computer. The computer schematic for this simulation is shown in figure 27. The command precompensator was formed by using a standard circuit for simulating a second-order lead-lag transfer function. The slew-rate limiter was implemented as a first-order lag with a saturation limiter on the velocity term. The power amplifier was modeled by an open-loop operational amplifier with a potentiometer in the feedback to achieve a high gain. Rather than using a diode function generator, the nonlinearity of the servovalve coil-current-to-coil-force gain was implemented by a limited signal being summed to the original signal. Both signals were passed through potentiometers to adjust the slopes of the curve. Stiction was modeled simply as a limited-spool velocity feedback term. Power-amplifier voltage and coil-current saturations were implemented with feedback limiters. The remainder of the simulation was a straightforward modeling of the equations used to form the block diagram of figure 10. Saturation levels were implemented to simulate controller operational amplifier saturation levels of 12 volts for the $K_e e_e$ and e_s signals. However, these levels were not encountered during a normal simulation run.

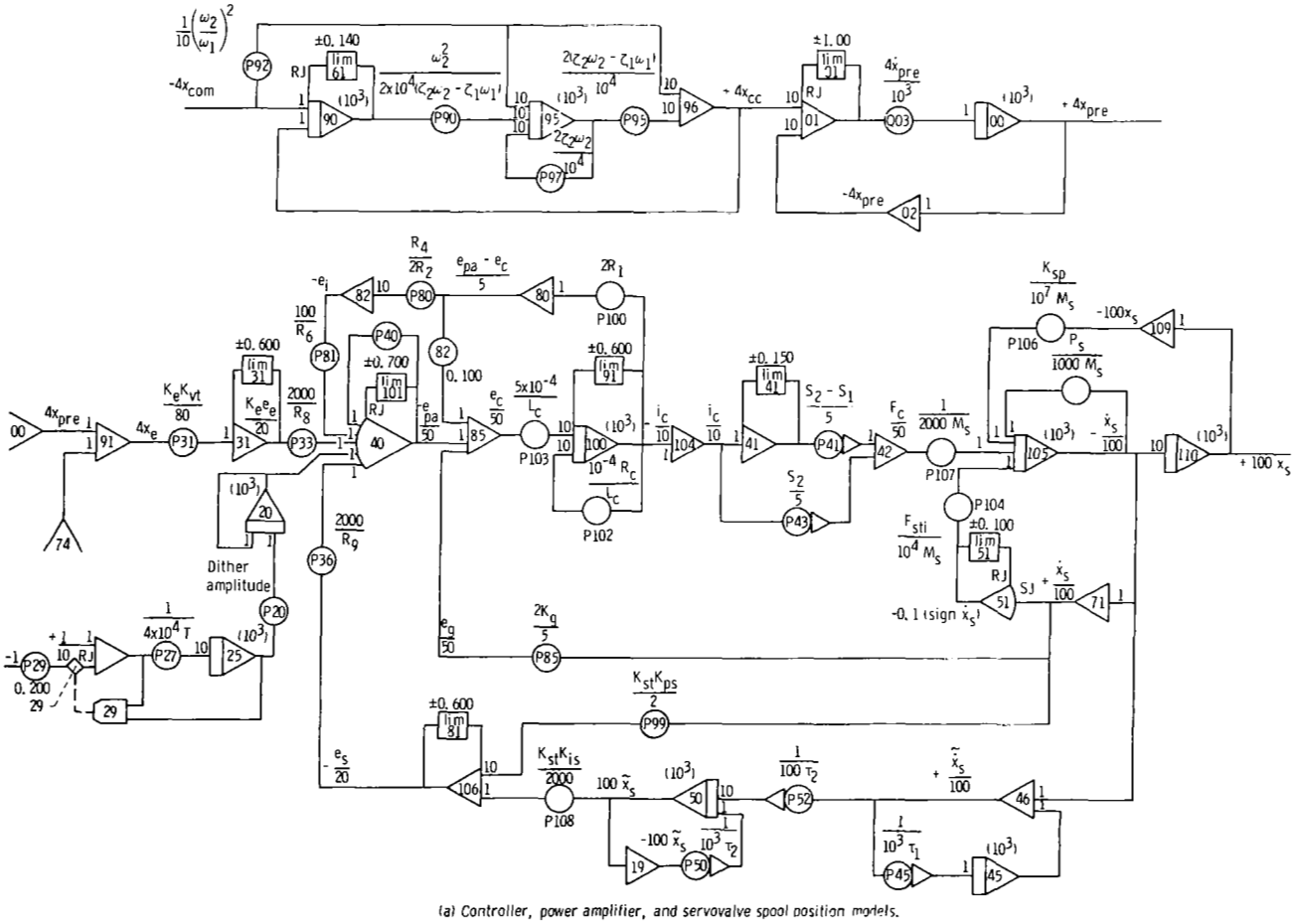

(a) Controller, power amplifier, and servovalve spool position models.

Figure 27. - Analog patching diagram for model of airflow-valve servosystem. (Scale factors are for U. S. customary units, e.g., lb and in.)

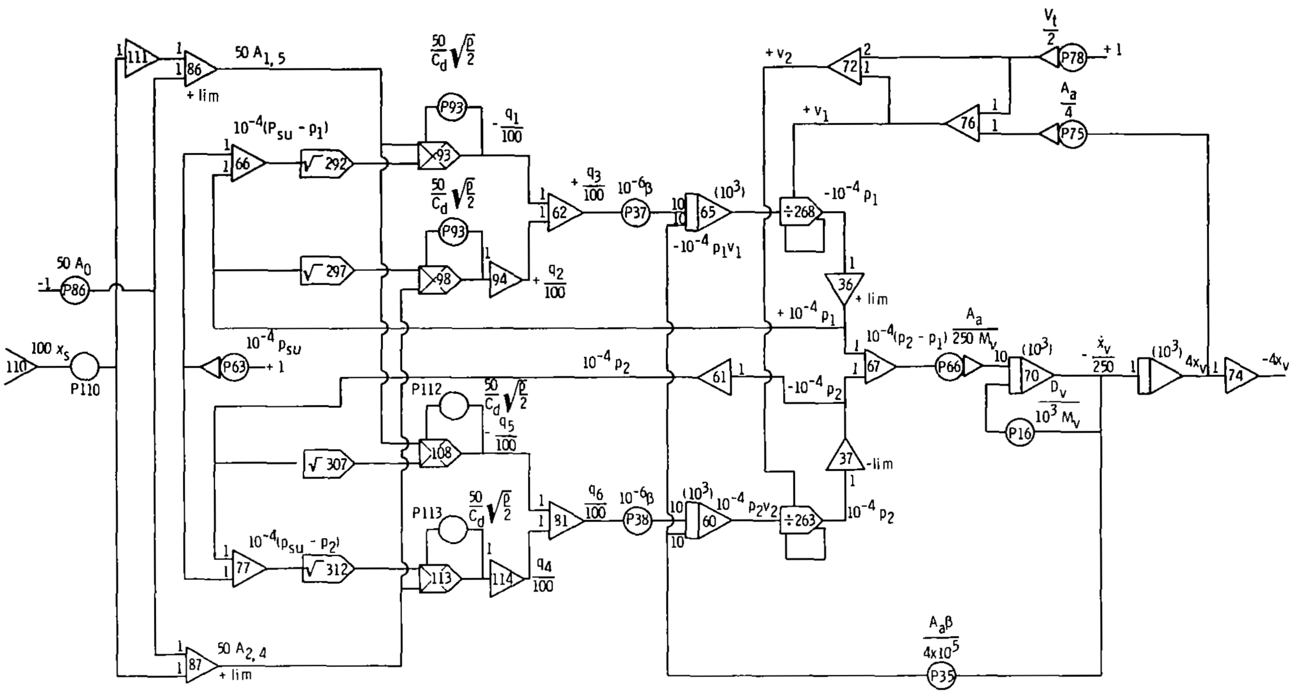

(b) Servovalve orifices and actuator models.

Figure 27. - Concluded.

Appendix C

Special Developmental Considerations

As is true of most equipment designs, unforeseen problems can occur during the initial hardware tests of a new device. This appendix discusses the problems encountered during preliminary testing of the airflow-valve prototype and its components and presents their solutions.

Spool Damping

The damping at the servovalve-spool, spring-mass resonant frequency was very light. Oscillations were readily excited by flow force noise. This problem was easily handled by the spool-velocity feedback, with the added advantage that the resonant frequency could be increased by generating a spool position signal and feeding it back. However, when the coil-current saturation was encountered, the damping generated by the velocity feedback term was lost for a portion of the cycle, and this modified the output waveform.

End-Cap Impact of Actuator Piston

The forces encountered with the actuator moving at full velocity and impacting one of the end caps can be destructive. To minimize the risk of such damage, two approaches were taken: A cushion mechanism was designed to minimize deceleration force levels. Or the controller was used to detect when the piston was approaching an end cap, and the servosystem gain was cut to slow the valve and shift the command toward a centered spool position. The concept of a hydraulic cushion had been employed in an earlier servosystem design (ref. 8); however, the cushion required additional piston travel and a volume penalty. Therefore, a cushion was implemented for the airflow-valve actuator by relying on the elastic spring characteristics of the bolts that hold the end caps to the actuator block.

The method used to minimize the deceleration force on impact was based on converting the kinetic energy of the moving mass into strain energy of deformation. The resulting stress in each member was kept below the yield point of the material in order to avoid permanent deformation. The amount of strain energy a member could absorb prior to permanent deformation was directly proportional to the yield point of the material squared and inversely proportional to the modulus of elasticity. Hence, when possible, materials with high yield points and low moduli of elasticity were chosen for the best resiliency. The strain energies of deformation of the end-cap bolts, the end cap, and the piston were considered. The compliance (reciprocal of the elastic spring constant) of the end-cap bolts was the major factor influencing the impact force level. The bolt length and diameter were thus sized to minimize the impact force. The unthreaded shank of each end-cap bolt was turned down to a diameter that was equivalent to the diameter of the tensile stress area of the screw threads so that the energy absorbtion would be equalized over the length of the bolt (fig. 7). If the bolts were made too compliant, the effects of the compliance had to be accounted for in determining the hydraulic resonance. It was necessary to maintain geometrical symmetry over the impacted area of the end cap in order to get equal energy absorption over the total region and to avoid local deformation.

The electronic method for avoiding end-cap impact was implemented in the servosystem controller by comparing the actuator position signal with reference levels equivalent to positions at either extreme of piston travel. If the piston travel exceeded these bounds, a latch was set and the forward-loop gain was decreased by a factor of 10. This gain drop would tend to center the servovalve spool and limit the amount of flow through the servovalve (as well as piston velocity). This method was useful as protection during preliminary servosystem response testing when controller gains were varied and occasional instability was encountered.

Actuator Position Transducer

To achieve the desired dynamic response for the actuator position signal, a linear, variable differential transformer (LVDT) was used with a synchronous demodulator type of signal conditioner (ref. 19). The carrier frequency was set to 20 kilohertz, and the demodulator filter was modified to contribute no more than 5° of phase at 1 kilohertz. The transducer was a hermetically sealed, double magnetically shielded device. The magnetic shielding was found to be necessary during early testing with an unshielded LVDT. The case became magnetized by the servovalve magnet and its output was distorted.

Using the airflow valve for compressor studies (fig. 3) placed the actuator in the area where turbine

exhaust flow exits. When the speed of the turbine was varied, the temperature of the expanding gases passing over the actuator block could vary considerably. To prevent the shift in accuracy (position feedback gain) that these temperature variations created in the LVDT signal, a pair of small heaters was mounted on the LVDT mounting block to maintain a constant temperature (fig. 5(a)).

Actuator-Piston Dynamics

During testing with the first prototype actuator, the piston seized during an 80 percent amplitude frequency sweep at a frequency of 205 hertz. The piston was driving a dummy mass load to simulate the airflow-valve moving element. Inspection of the hardware showed that the piston lands had touched the inside bore of the actuator block. Discoloration of the end caps indicated a possible lubrication problem. Further tests with proximity probes to measure the horizontal and vertical positions of the dummy mass indicated that the problem was due to a structural mode of the actuator piston. Figure 28 shows a sketch of the bending motion that the piston may have been experiencing. To determine the frequency of this mode, impact tests of the dummy mass were performed. (The piston was centered and the hydraulic chambers were pressurized.) The resulting position transient, along with a frequency reference signal, was recorded with a digital transient recorder. The result, shown in figure 29(a), was a resonant frequency of 410 hertz, which was twice the frequency of excitation at which the piston seized.

To demonstrate that a subharmonic excitation frequency could excite the structural mode, the piston was actuated at a low amplitude (10 percent of full stroke) with a frequency of 210 hertz. The result is shown in figures 29(b) and (c), a time trace of the proximity probe outputs and an X-Y plot of load mass motion, respectively. Although the horizontal motion consisted primarily of the excitation frequency (with the actuator control-port flows impinging on the piston horizontally), the vertical motion clearly show the higher frequency at twice the excitation value. Had the excitation stroke amplitude been larger, this higher frequency amplitude could have reached a level where the bending of the piston rod would exceed allowable clearances and cause the failure observed earlier.

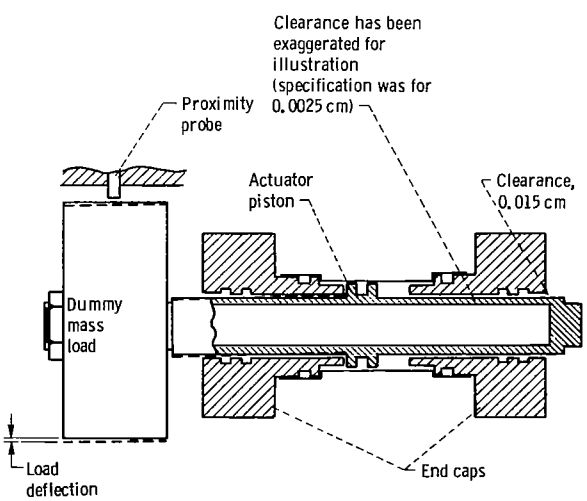

Figure 28. - Possible structural mode of actuator piston.

This determination resulted in a redesign of the actuator. The piston shaft diameter was increased from 1.74 centimeters to 3.18 centimeters to increase the stiffness and vibrational frequency. Although excitation of this higher frequency by subharmonics could still not be completely avoided during sweep testing, the increased stiffness insured that the resulting amplitudes were small enough to be within specified clearances. Some weight penalty was encountered with the larger diameter piston, but it was small relative to the load mass of the airflow-valve moving element. Oil feed grooves were added to the end caps to insure good lubrication and to avoid the high temperatures encountered earlier.

The presence of airflow-valve motion in a direction perpendicular to the piston axis created an additional problem since this would have allowed the valve moving element to contact its fixed element and lead to excessive wear, or galling. Since the clearance between these two cylinders was set by the leakage specifications, it could not be increased to avoid this problem. The solution was the flame-sprayed lubricant coating discussed in the main text, in the section *Airflow-valve design*. The coating allowed contact with no damage and avoided the necessity for any additional load-bearing devices on the airflow-valve moving element.

ServoActuator Mount Dynamics

The initial tests to evaluate the servosystem were performed with a floor-mounted arrangement, as shown in figure 1. However, using this device for compressor studies required that it be mounted on a structure that was supported by a large cantilevered beam (fig. 3). This mounting arrangement was dictated by the existing equipment in the large-altitude-tank test facility in which the compressor tests were conducted. When the servosystem was mounted in this manner, reaction forces at the base of the actuator excited a structural resonance. A plot of the amplitude frequency response for the actuator-piston position, commanded to move at 10 percent of

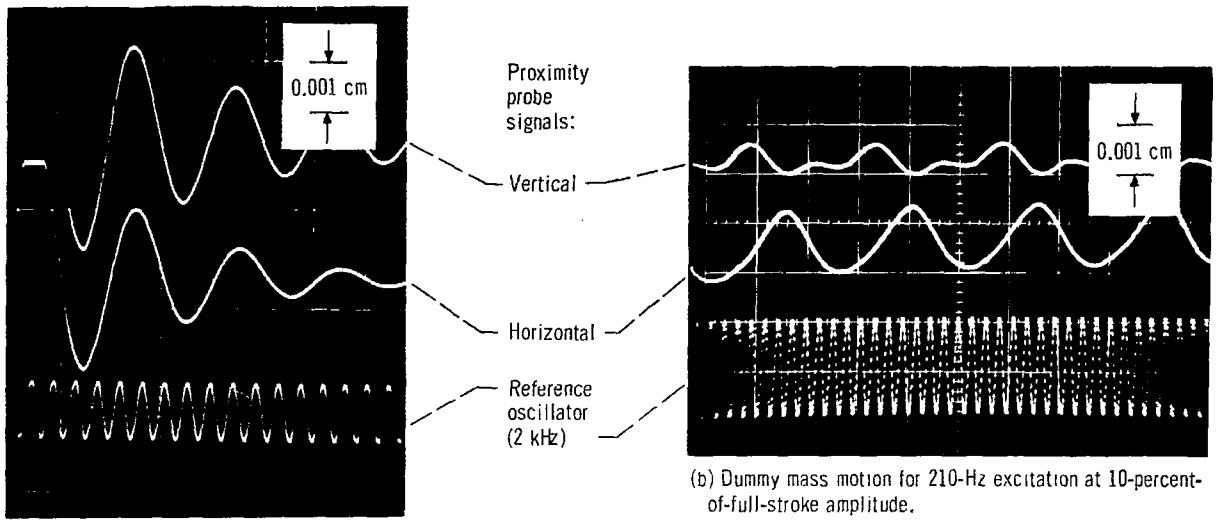

(a) Results of impact test with piston centered and system under pressure.

(b) Dummy mass motion for 210-Hz excitation at 10-percent-of-full-stroke amplitude.

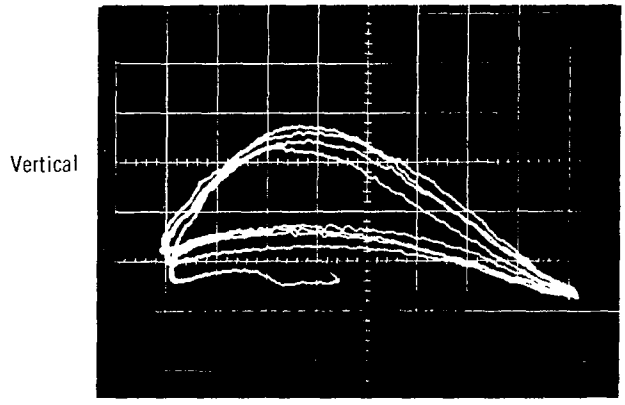

(c) X-Y plot of dummy mass motion for (b).

Figure 29. - Results of investigation into structural resonant mode of early airflow-valve piston design that used proximity probes to measure motion of a dummy mass load.

full stroke, is presented in figure 30 for both the floor-mounted and stand-mounted cases. The peak at about 210 hertz results from the vertical stand vibrations moving the servovalve case relative to the spool. This motion created an additional relative spool motion beyond that being commanded by the error signal. Since the total stroke of the spool was only ±0.020 centimeter, small motions of the servovalve case could create appreciable changes in the flow through the spool orifices.

This problem was partially eliminated by mounting an accelerometer (fig. 5(a)) on the servovalve case and feeding its signal back through the controller. The accelerometer signal was integrated twice with the circuit available in its signal conditioner to provide a case position signal. Since this integration has a high gain at low frequency, the position output from the signal conditioner was high-pass filtered before being summed into the actuator-position error signal. The gain of this feedback was set experimentally by increasing its value until the resonant peak at 210 hertz was minimized. In effect, the acceleration feedback provided a signal for adjusting the spool motion to maintain its position relative to the servovalve case by using the actuator-position error signal. The technique worked well but did not completely eliminate the effect of case vibrations.

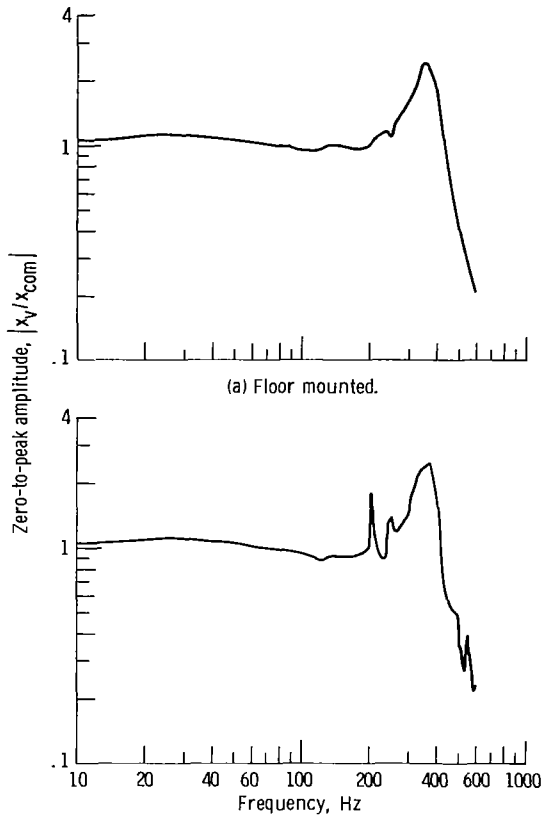

(a) Floor mounted.

(b) Test-stand mounted, without accelerometer feedback.

Figure 30. - Effect of mount dynamics on servosystem response.

References

1. Baumbick, Robert J.; Neiner, George H.; and Cole, Gary L.: Experimental Dynamic Response of a Two-Dimensional, Mach 2.7, Mixed Compression Inlet. NASA TN D-6957, 1972.
2. Baumbick, Robert J.; et al.: Dynamic Response of Mach 2.5 Axisymmetric Inlet with 40 Percent Supersonic Internal Area Contraction. NASA TM X-2833, 1973.
3. Milner, Edward J.; Wenzel, Leon M.; and Paulovich, Francis J.: Frequency Response of an Axial-Flow Compressor Exposed to Inlet Pressure Perturbations. NASA TM X-3012, 1974.
4. Cole, Gary L.; Cwynar, David S.; and Geyser, Lucille C.: Wind-Tunnel Evaluation of the Response of a YF-12 Aircraft Flight Inlet to Internal Airflow Perturbations by Frequency-Response Testing. NASA TM X-3141, 1974.
5. Baumbick, Robert J.: Device for Producing Dynamic Distortion Patterns at Inlets of Air-Breathing Engines. NASA TM X-2026, 1970.
6. Cole, Gary L.; Neiner, George H.; and Baumbick, Robert J.: Terminal Shock Position and Restart Control of a Mach 2.7, Two-Dimensional, Twin Duct Mixed Compression Inlet. NASA TM X-2818, 1973.
7. Neiner, George H.; Arpasi, Dale J.; and Dustin, Miles O.: Wind-Tunnel Evaluation of YF-12 Aircraft Inlet Control System by Frequency-Response and Transient Testing. NASA TM X-3142, 1975.
8. Webb, John A., Jr.; Mehmed, Oral; and Hiller, Kirby W.: Improved Design of a High-Response Slotted Plate Overboard Bypass Valve for Supersonic Inlets. NASA TM X-2812, 1973.
9. Zeller, John R.: Analysis of Dynamic Performance Limitations of Fast Response (150 to 200 Hz) Electrohydraulic Servos. NASA TN D-5388, 1969.
10. Zeller, John R.; and Webb, John A., Jr.: Determination and Evaluation of Performance Limit Criteria of Fast-Response Electrohydraulic Servosystems. NASA TM X-2736, 1973.
11. Steffen, Fred W.; et al.: A Turbojet Simulator for Mach Numbers up to 2.0. NASA TM X-67973, 1972.
12. HV-40 High Performance Industrial Servo Valve. Bulletin I-5000, MB Electronics Division, Gilmore Industries, Inc., 1968.
13. Sliney, Harold E.: Plasma-Sprayed, Metal-Glass and Metal-Glass Fluoride Coatings for Lubrication to 900° C. NASA TM X-71432, 1973.
14. Sliney, Harold E.: Plasma-Sprayed, Self-Lubricating Coatings for Use from Cryogenic Temperatures to 870° C (1600°F). NASA TM X-71798, 1975.
15. Merritt, Herbert E.: Hydraulic Control Systems. John Wiley & Sons, Inc., 1967.
16. Thayer, W.J.: Transfer Functions for Moog Servovalves. Tech. Bull. No. 103, Moog Servocontrols, Jan. 1965.
17. de Pennington, A.; 't Mannetje, J.J.; and Bell, R.: The Modeling of Electrohydraulic Control Valves and Its Influence on the Design of Electrohydaulic Drives. J. Mech. Eng. Sci., vol. 16, no. 3, June 1974, pp. 196-204.
18. Webb, John A., Jr.; and Blech, Richard A.: Predicting Dynamic Performance Limits for Servosystems with Saturating Nonlinearities. NASA TP-1488, 1979.
19. Herceg, Edward E.: Handbook of Measurement and Control. Schaevitz Engineering, 1972.

1. Report No. NASA TP-1678	2. Government Accession No.	3. Recipient's Catalog No.
4. Title and Subtitle SINGLE-STAGE ELECTROHYDRAULIC SERVOSYSTEM FOR ACTUATING AN AIRFLOW VALVE WITH FREQUENCIES TO 500 HERTZ		5. Report Date August 1980 6. Performing Organization Code
7. Author(s) John A. Webb, Jr., Oral Mehmed, and Carl F. Lorenzo		8. Performing Organization Report No. E-252 10. Work Unit No. 505-05
9. Performing Organization Name and Address National Aeronautics and Space Administration Lewis Research Center Cleveland, Ohio 44135		11. Contract or Grant No. 13. Type of Report and Period Covered Technical Paper
12. Sponsoring Agency Name and Address National Aeronautics and Space Administration Washington, D.C. 20546		14. Sponsoring Agency Code

15. Supplementary Notes

16. Abstract

An airflow valve and its electrohydraulic actuation servosystem are described. The servosystem uses a high-power, single-stage servovalve to obtain a dynamic response beyond that of systems designed with conventional two-stage servovalves. A detailed analysis of the electrohydraulic servosystem is presented, along with a discussion of the limitations imposed on system performance by such nonlinearities as signal saturations and power limitations. Also included are descriptions of the mechanical design concepts and developmental considerations. Dynamic data are presented in the form of sweep-frequency test results. These data are compared with analytical results obtained with an analog computer model. Good agreement was obtained for a wide range of excitation amplitudes.

17. Key Words (Suggested by Author(s))	18. Distribution Statement
Electrohydraulic servosystem; Servosystem; Servovalve; Fast-response system; Nonlinear; Saturation; Analysis; Control	Unclassified – Unlimited Subject Category 08

19. Security Classif. (of this report)	20. Security Classif. (of this page)	21. No. of Pages	22. Price*
Unclassified	Unclassified	34	A03

* For sale by the National Technical Information Service, Springfield, Virginia 22161

NASA-Langley, 1980